國立交通大學

資訊科學與工程研究所

碩士論文

運用多台 KINECT 對汽車周遭做立體監控

3D Monitoring of Car Surrounds Using Multiple KINECT Devices

研究生：黃浩哲

指導教授：蔡文祥　教授

中華民國一百零二年六月

運用多台 KINECT 對汽車周遭做立體監控

3D Monitoring of Car Surrounds Using Multiple KINECT Devices

研 究 生：黃浩哲　　Student：Hao-Che Huang

指導教授：蔡文祥　　Advisor：Wen-Hsiang Tsai

國 立 交 通 大 學

資 訊 科 學 與 工 程 研 究 所

碩 士 論 文

A Thesis

Submitted to Institute of Computer Science and Engineering

College of Computer Science

National Chiao Tung University

in partial Fulfillment of the Requirements

for the Degree of

Master

in

Computer Science

June 2013

Hsinchu, Taiwan, Republic of China

中華民國一百零二年六月

3D Monitoring of Car Surrounds Using Multiple KINECT Devices

Student: Hao-Che Huang Advisor: Wen-Hsiang Tsai

Institute of Computer Science and Engineering

National Chiao Tung University

ABSTRACT

In this study, several methods are proposed for 3D monitoring of car surrounds using multiple KINECT devices affixed around a video surveillance vehicle. Around-car object models are constructed with 3D sensing techniques provided by KINECT devices. Based on the constructed models, an around-car monitoring system for car-accident warning and avoidance is developed.

Firstly, a method for coordinate conversion based on the pinhole camera model is proposed, which converts the coordinates of the depth image into 3D space points. The method is then used to construct 3D images from the color and depth images acquired with KINECT devices. Also, a geometric correction scheme is employed to correct the bending phenomenon of constructed 3D images. Next, a method for KINECT device calibration using the iterative closest point (ICP) algorithm is proposed, which is used to stitch the 3D images corresponding to the around-car KINECT devices into an around-car 3D image. And by the use of the 3D DWC measure which is an extension of the 2D DWC, the displacements between the 3D images of neighboring KINECT devices are computed, by which a more complete by-passing car model can be constructed and car-accident scenes can be restored.

Furthermore, a method for monitoring and computing parameters related to ramps and height-restricting barriers is proposed, which uses trigonometric functions and mathematical geometry to measure the slopes of ramps and calculate the height difference between the car roof and the barrier for pre-warning of possible car collisions. Finally, in order to increase driving safety, a method for predicting the possible direction and movement of the opposite car is proposed.

Good experimental results are also shown, which prove the feasibility of the proposed methods for real applications.

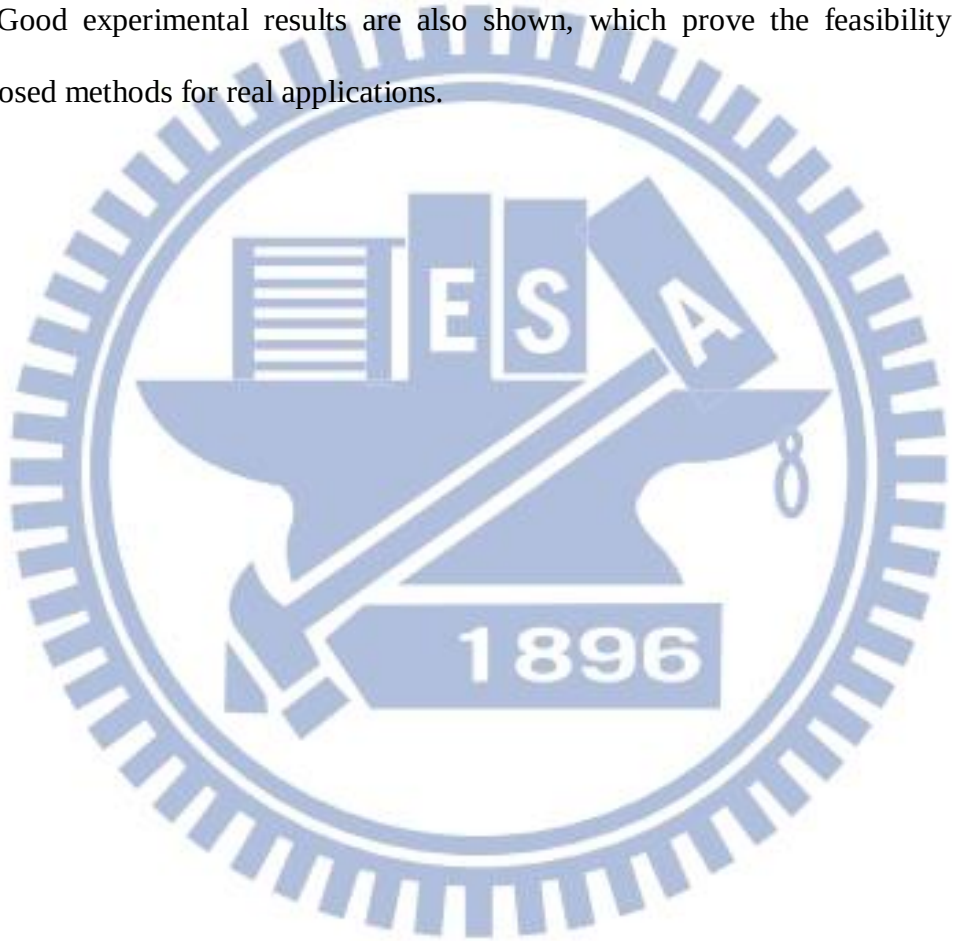

運用多台 KINECT 對汽車周遭做立體監控

研究生：黃浩哲　　指導教授：蔡文祥 博士

國立交通大學資訊科學與工程研究所

摘要

本研究提出數項利用架設在視訊監控車周圍的 KINECT 裝置，對汽車周遭環境做立體監控的方法。該等方法運用 KINECT 裝置提供的 3D 感測技術建立環車物體模型，再藉由這些模型開發環車監控系統，用於提醒駕駛人車遭狀況，避免車禍意外發生。

首先，基於針孔成像原理，本研究利用座標轉換將深度影像轉換至 3D 空間，之後把 KINECT 裝置取得的深度與彩色影像統整成一 3D 影像，同時採用幾何方法修正 3D 影像的彎曲現象。接著，基於遞迴最近點(iterative closest point, ICP)的觀念提出一校正 KINECT 裝置的方法，將各個環車 KINECT 裝置的 3D 影像接合成一完整的環車立體影像。另外，使用從二維的距離加權相關係數(2D distance-weighted correlation, 2D DWC)延伸出來的 3D DWC，計算出 3D 影像間的位移，完整地建立從旁經過汽車的模型，並還原車禍事故現場。

最後，提出一對於路面斜坡和限高障礙物做監控和計算參數的方法，該方法使用三角函數和幾何數學，測量路面斜坡的坡度，並推算車頂和限高障礙物的高度差，以預先提醒駕駛人避免碰撞。另為增進道路駕駛安全，亦提出一針對對向汽車預測可能行進方向與移動的方法。

上列方法的實驗結果良好，顯示出本研究所提系統確實可行。

ACKNOWLEDGEMENTS

The author is in hearty appreciation of the continuous guidance, discussions, and support from his advisor, Dr. Wen-Hsiang Tsai, not only in the development of this thesis, but also in every aspect of his personal growth.

Appreciation is also given to the colleagues of the Computer Vision Laboratory in the Institute of Computer Science and Engineering at National Chiao Tung University for their suggestions and help during his thesis study.

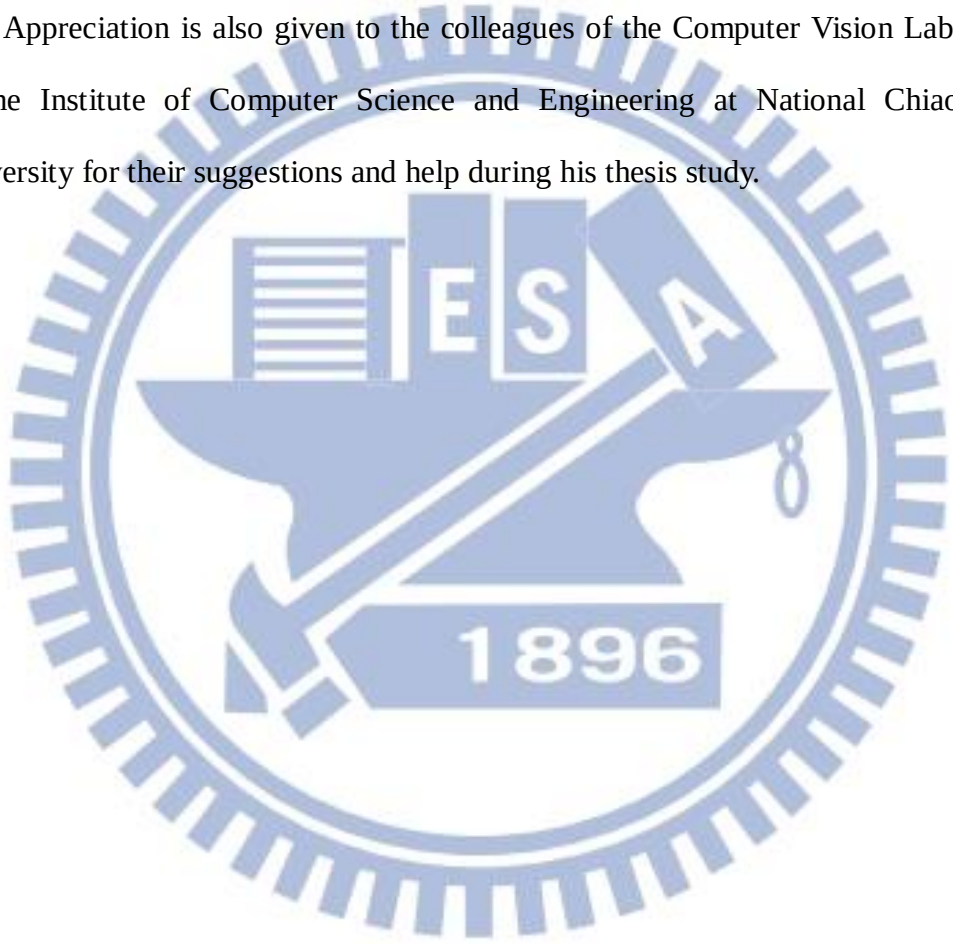

CONTENTS

LIST OF FIGURES

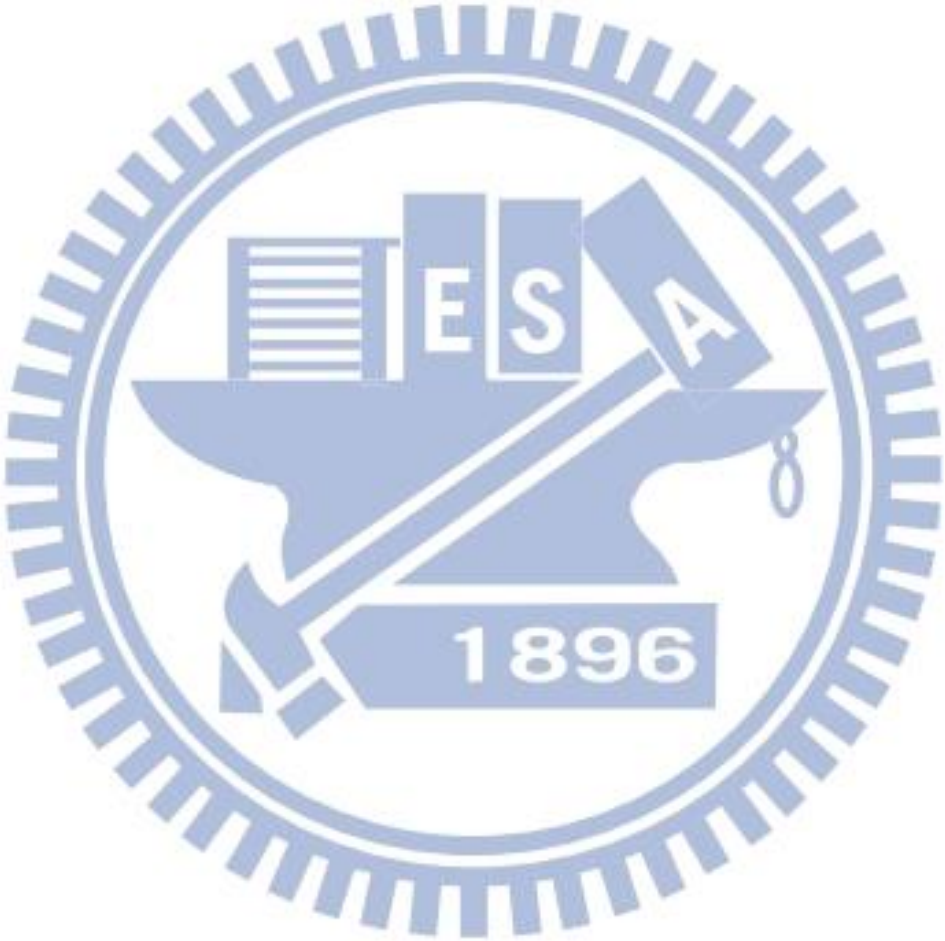

LIST OF TABLES

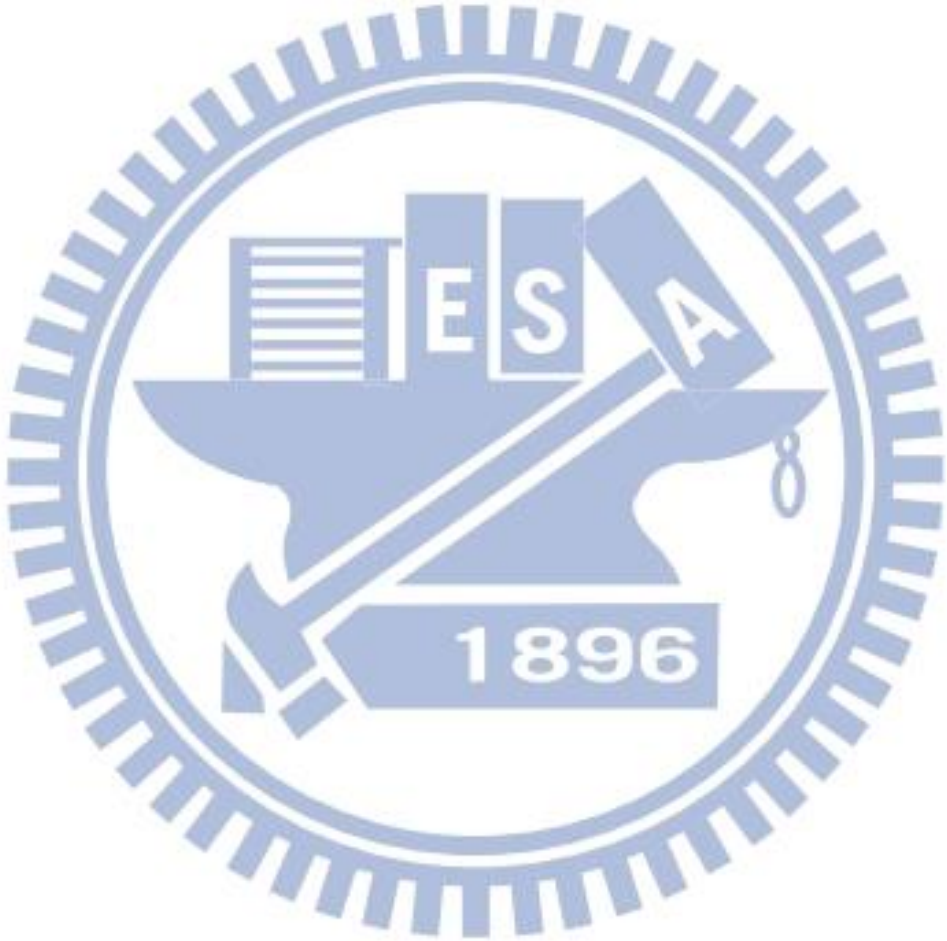

Chapter 1
Introduction

1.1 Background and Motivation

With the increase of communications and the growth of populations, the frequency of traffic accidents increases year by year with a fast speed. If a traffic accident occurs on a highway in crowded commuting hours, a lot of costs will be spent for the community to rescue the injured people and reduce the traffic jam. Starting with this motivation, in this study we try to use new 3D sensing equipments to improve driving safety and to detect blind areas around the car. It is desired to design not only a more stable around-car monitoring system but also innovative methods for around-car object detection.

The KINECT device is produced by Microsoft for playing somatosensory games. It can capture players' movements and react to the game condition. By using the 3D depth sensor and the RGB camera built in the KINECT device, we can acquire color and depth images at the same time from which we can create 3D images and construct object models. Therefore, it is desired to affix multiple KINECT devices around the vehicle to detect around-car dangerous events in this study.

Around-car information is important in the designs and applications of intelligent vehicles. Different to traditional methods of 2D around-car sensing using traditional perspective cameras, in this study we will use 3D sensing techniques provided by KINECT devices to acquire color and depth images and construct accordingly around-car object models. And based on the use of the constructed model, we will

develop new methods and apply them to develop an around-car monitoring system for car-accident warning and avoidance.

1.2 Review of Related Works

About the related works of around-car monitoring, Scharfenberger et al. [1] designed a detection system for safe opening of car doors. In that research, they affix a camera to the rear-view mirror of the front door. The camera keeps acquiring around-car scenes, learning background scenes, detecting objects, and separating foreground objects from background images. When a passenger or a driver opens a car door, systematic detection of the around-car situations is conducted continuously to confirm whether there is a person too close to the car door.

In the research of Gandhi and Travedi [2], two surrounding cameras are affixed to the rear-view mirrors of the car, one on each side; and a system for around-car object detection was constructed. In the system, because the two cameras they used can shoot front scenes at the same time, the distance of the front object to the car can be computed by a method of 3D vision processing.

In the application of 3D sensing, a research team led by Archarya in Canesta Company designed a 3D sensor for assisting car parking [3]. They defined a detective area which people concern the most when parking the car. The research team designed a sensor for distance measuring by the technique of time differencing, which is energy-saving, anti-glare, and suitable to detect pedestrians and obstacles.

Liu et al. [4] affixed six fish-eye cameras to the car around to sense around-car scenes seamlessly. Each fish-eye image is distortion-corrected and is connected to another by image stitching. Because every camera’s level of distortion and condition of lighting in image taking are different, they eliminated the joints and changes of

brightness during the image stitching process. In this way, an around-car image is constructed. In short, the system acquires around-car scenes by fish-eye cameras and constructs an around-car image from the top view in order to help the driver during driving ahead and astern.

Chaiyawatana et al. [5] used the frame subtraction technique to construct a system which detects by-passing objects automatically. The objects' movements in the image are detected if the difference value resulting from frame subtraction exceeds a pre-selected threshold.

1.3 Overview of Proposed Methods

In this study, we set up a new KINECT-based around-car monitoring system by installing a number of KINECT devices (14 ones) around a vehicle as a platform for monitoring the car surround. A picture of the vehicle with installed KINECT devices is shown in Fig. 1.1

(a) (b)

Figure 1.1 Proposed KINECT-based around-car monitoring system (with 14 KINECT devices) installed on a vehicle. (a) The vehicle. (b) An installed KINECT device.

As shown in Fig. 2, the first major task of the proposed system is construction of 3D images from KINECT images (including color and depth images). At first, we convert coordinates between different coordinate systems. The unit of KINECT images is pixel, so we convert it, by using the pinhole camera model, into millimeter which is the unit of 3D images. Then, we try to solve the problem that the shape of the scene captured from the KINECT device is "fanned." The reason why this problem arises is that the infrared light rays sent out by the KINECT device for depth sensing do not go in parallel. To solve the problem, we introduce a method for geometric correction of 3D images.

The second major task of the proposed system is modeling of around-car events. For this, at first we calibrate the "geometric relation" between every two neighboring KINECT devices. The iterative closest point (ICP) scheme is adopted for this purpose here. After the calibration work, merging 3D images from neighboring KINECT devices is conducted. For this, we propose a method of using a new similarity measure, 3D distance-weighted correlation (DWC), for 3D image matching and integration, in order to model by-passing cars and to restore car-accident scenes. During image matching, the 3D DWC measure is used to compute the 3D displacement between two sequential 3D images. Then, sequential 3D images are overlapped according to the found displacements. In this way, objects in different frames can be overlapped accurately at appropriate positions, yielding a complete by-passing car model. Similarly, as we try to restore a car-accident scene, we compute the models of the involved cars which appear just before the car collision happens. The responsibility of the car accident can so be clarified by inspecting the relative geometric conditions of the constructed car models.

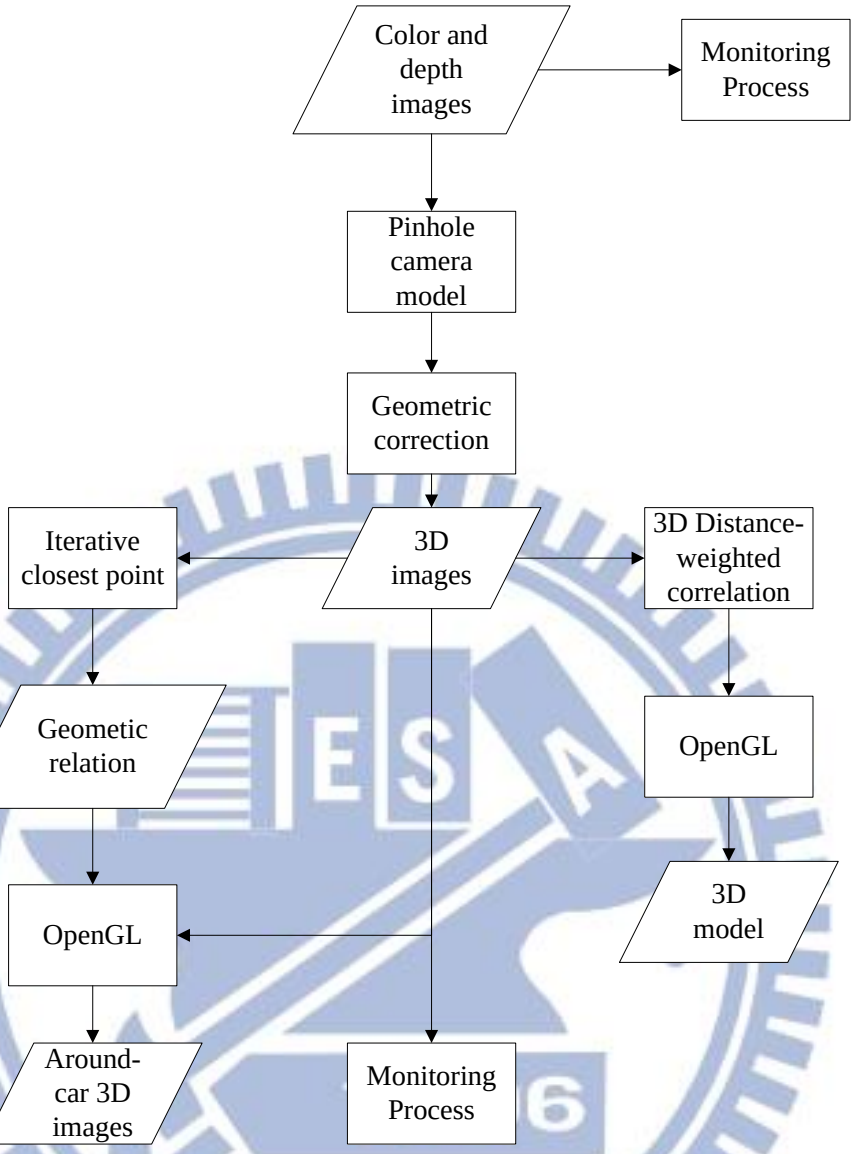

Figure 1.2 Major tasks of proposed KINECT-based around-car monitoring system.

The last task conducted by the proposed system is computation of the real-time response to around-car dangerous events. We identify three cases for this purpose. In the first two cases, a method of using trigonometric functions to measure the slope of the ramp in front of the car and the height of the obstacle nearby is proposed. The third case is pre-warning of possible car collisions to assist safe driving. In this case, a linear prediction equation is adopted to compute the current speed and direction of the

nearby car and to predict possible collisions for driving adjustment.

1.4 Contributions

The major contributions of this study are listed in the following.

1. A new KINECT-based around-car monitoring system is proposed to *monitor* the car surrounds to satisfy the demands of driving safety.
2. A 3D DWC-based method is proposed to *calibrate* the geometric relations between two KINECT devices.
3. A method is proposed to construct *3D images* in the real-world space.
4. Another 3D DWC-based method is proposed for matching 3D images to construct by-passing *car models*.
5. A method is proposed to model *around-car events* for clarifying the responsibility of car accidents.

1.5 Thesis Organization

The remainder of this thesis is organized as follows. In Chapter 2, we introduce the configuration of the proposed system and the system processes in detail. In Chapter 3, the method for constructing 3D images is described. In Chapter 4, we introduce the proposed methods for image matching based on the 3D DWC and modeling of around-car events. In Chapter 5, we describe the proposed methods for real-time response to around-car dangerous events. The details include monitoring of ramps, monitoring of limitations of heights, and computation for collision-avoiding driving. In Chapter 6 experimental results and discussions are presented. Finally, conclusions and some suggestions for future works are given in Chapter 7

Chapter 2
System Design and Processes

2.1 Ideas of Proposed System

Because of the need for around-car imaging and monitoring in this study, we affix multiple KINECT devices to the car body, as shown in Figure 2.1. After reading the image data collected by the devices, we realized that the data of four KINECT devices affixed around the car as shown in Figure 2.1(a) are not enough to cover the entire car surround because the horizontal viewing angle of a KINECT device is only 57 degrees. In order to collect complete around-car information, the number of the KINECT devices affixed to the car body is increased to be 14 later in this study. In order to acquire data from the front top of the car, we also affix one more KINECT device to there. So, totally 15 KINECT devices are affixed to the vehicle used in this study.

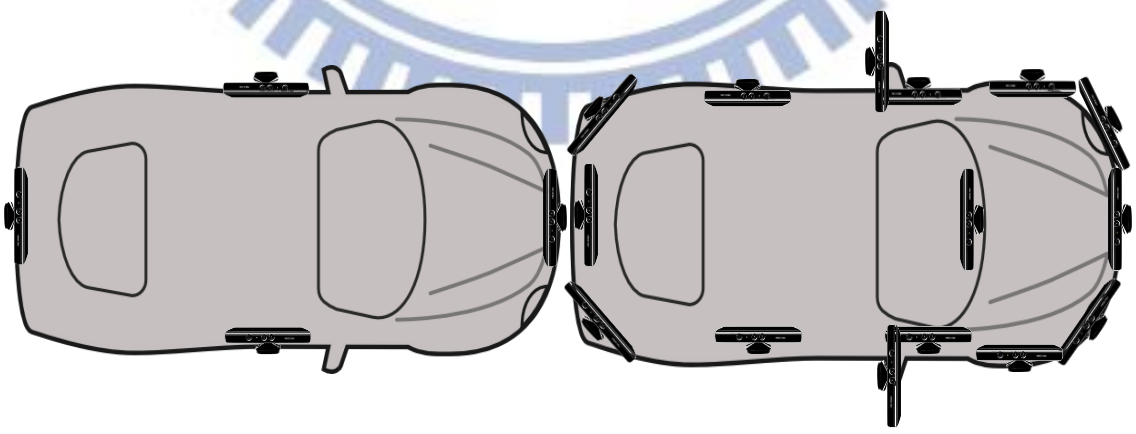

(a) (b)

Figure 2.1 Proposed KINECT-based around-car monitoring system installed on a vehicle. (a)With 4 KINECT devices. (b) With 15 KINECT devices.

In more detail, in the proposed system a KINECT device occupies a USB port of the laptop or desktop computer used as the controller of the proposed monitoring system. Although one laptop or desktop computer contains lots of USB ports, the hardware and speed limitations of the controller computer do not allow too many KINECT devices to work simultaneously because every KINECT device need be connected to a distinct USB port. Normally, a desktop computer contains two USB controllers while a laptop contains only one. In order to increase the number of USB ports without using more computers, a USB expansion card is used. As a result, nine KINECT devices can work simultaneously using one computer as the host. In Section 2.2, we will describe the configuration of the proposed system, including the hardware and software. The system processes, including the learning process and the monitoring process, will be described in Section 2.3.

2.2 System Configuration

In order to record and monitor around-car conditions, KINECT devices are affixed to the car body. A SDK for acquiring color and depth information and a software program for displaying the collected data is needed besides the KINECT devices. In Section 2.2.1, we introduce hardware equipment, including iron brackets of the KINECT devices, the desktop computers used for experiments, and the structure of the KINECT device, etc. In Section 2.2.2, some software, including the OpenNI, the OpenGL, and the used programming language are introduced.

2.2.1 Hardware Configuration

At first, we introduce the protagonist — the KINECT device. It includes a color

VGA video camera, a depth sensor, a multi-array microphone, and a motor for tilting the device. The hardware specifications of the KINECT device [6] are sorted and listed in Table 2.1. The appearance of the KIENCT device [7] is shown in Figure 2.2. In this section, some experiences obtained during using KINECT devices in this study are described. From Table 2.1, we can see that the range of the depth sensor is 1.2 to 3.5 meters. In fact its working range is larger, from 0.8 to about 6.0 meters. In addition, the accuracy of the depth image is millimeter. The tilt range of KINECT device is ±27 degrees. In fact, the KINECT device can tilt for about 30 degrees according to our real test results.

Table 2.1 Hardware specifications of a KINECT device.

Horizontal viewing angle	57 degrees
Vertical viewing angle	43 degrees
Tilt range of the device	±27 degrees
Range of the depth sensor	1.2-3.5 meters
Resolution of color images	640 x 480
Resolution of depth images	320 x 240

Next, the desktop computer used as the monitoring controller is introduced. The processor is an Inter Core i7-3770 Quad-core CPU with a Transcend DDR3 16G RAM; and the graphics card is of model Gigabyte GV-R7750C 2GI. We choose to use such a powerful processor and so big memory in order to use the processor to analyze lots of image data.

Furthermore, iron brackets are introduced, which were designed for holding the KINECT devices around the car, as shown in Figure 2.3. Three bases are affixed to each of the four sides of the car, and two bases are affixed onto the rear-view mirrors

of the car, one on each side, as shown in Figure 2.4.

Figure 2.2 Appearance of the KIENCT device.

(a) (b)

Figure 2.3 A base for the KINECT device (a)Without a KINECT device. (b) With a KINECT device.

(a) (b)

(c) (d)

Figure 2.4 Around-car bases (a) A front view. (b) A back view. (c) A lateral view. (d) A rear-view mirror.

2.2.2 Software Configuration

In the software configuration, we first introduce one of the SDKs of the KINECT device — OpenNI. OpenNI is the open source which enables the KINECT device to work on a computer and help us to acquire color and depth information captured from KINECT devices. Furthermore, it drives the motor in the KINECT device for the purpose of adjusting the angle of elevation.

OpenGL is also an open source which provides libraries to draw points in the 3D space. Thus, we can display constructed 3D images easily, as shown by the example in Figure 2.5.

Figure 2.5 A 3D image drawn by OpenGL.

Last, we introduce the programming language and development tool used in our program. The common C language, C++, is used as our programming language in order to be consistent with that use in the library of OpenNI. The adopted development tool is also the common *Microsoft Visual Studio 2010*, which is used as the compiler of the program.

2.3 System Processes

2.3.1 Learning Process

Before the monitoring process, a learning process is necessary. To merge 3D

images taken by neighboring KINECT devices, calibrating the relationship parameters of the devices are needed. Regarding the fact that a KINECT device is able to tilt in vertical direction, at the beginning of the calibration process, we use the libraries of OpenNI to adjust the device angle by controlling its motor to make sure its direction is parallel to the ground. Then, an ICP scheme is adopted for computing the horizontal angle and the displacement of the device with respect to its neighboring one.

Another task of learning is computing the environmental parameters. When driving on the road with different widths, setting different thresholds to filter out unrelated scenes is needed to obtain the monitoring target accurately. And we do this in our learning process as well. A flowchart of the proposed learning process is shown in Figure 2.6.

2.3.2 Monitoring Process

While driving on the road, once a ramp is discovered, the slope in degrees of the ramp will be displayed by the system as a warning to the driver. The system will also notify the driver a signal about whether to pass the ramp or not when driving to a place with a limitation on the car height, such as at the entrance of a parking lot, while going through a road under a bridge, etc. Furthermore, the driver is notified as well whether a car collusion is going to happen while encountering a by-passing car. Finally, after the car is parked, the system is used in an offline fashion to model around-car scenes, and analyze them to check the responsibility if legal cases about car accidents arise. A flowchart of the monitoring process is shown in Figure 2.7.

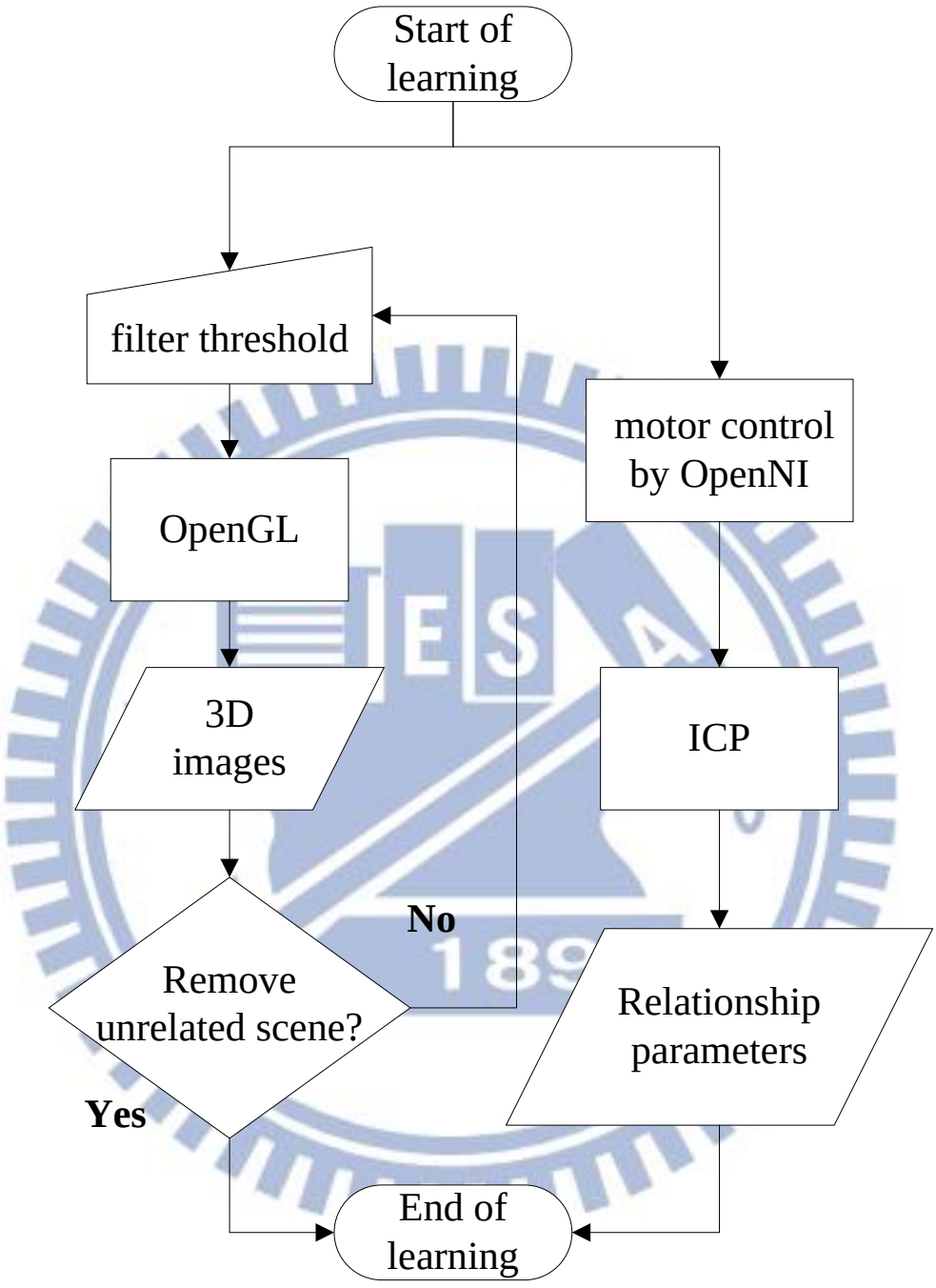

Figure 2.6 A flowchart of the learning process.

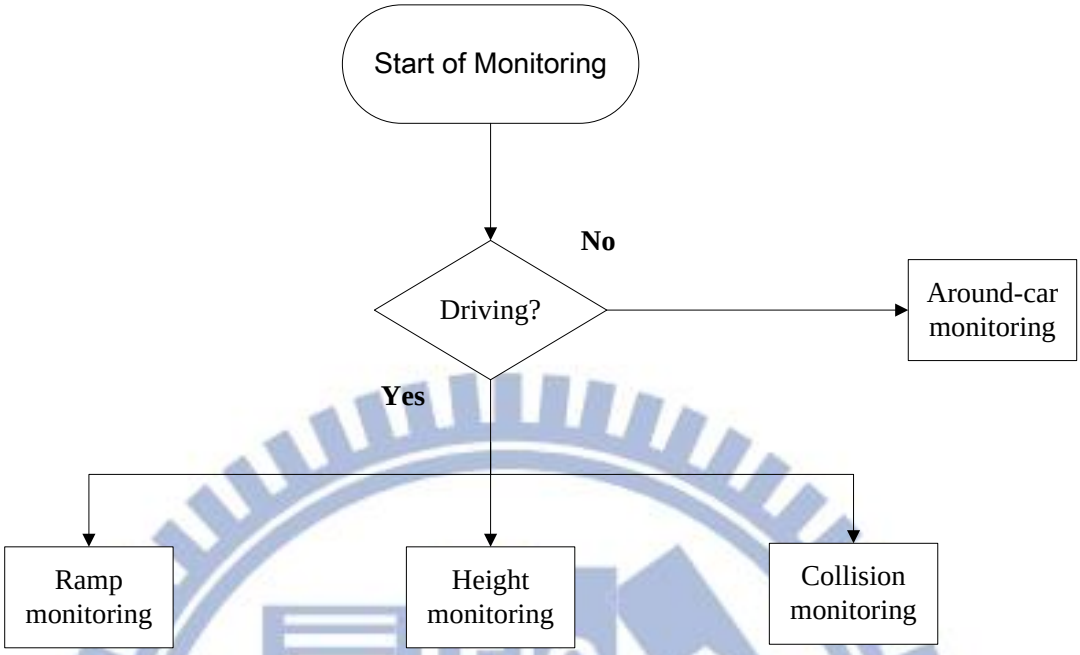

Figure 2.7 A flowchart of the monitoring process.

Chapter 3
Construction of 3D Images from KINECT Images

3.1 Review of Pinhole Camera Model

The *pinhole camera* is a simple camera model with an aperture of only the pinhole size. It may be regarded as an opaque box with a pinhole on one side. The light passing the pinhole will produce an upside-down projection of the scene in front of the pinhole, as illustrated in Figure 3.1 [8].

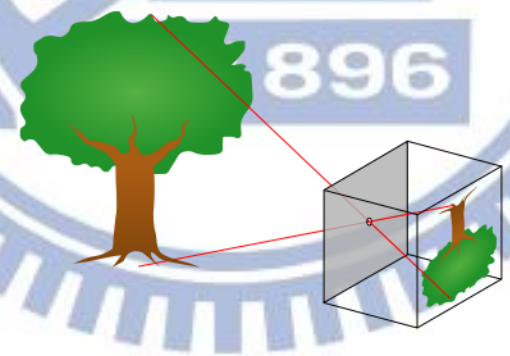

Figure 3.1 An illustration of a pinhole camera model.

The pinhole camera model describes the mathematical relationship between a 3D point and its projection on the image plane of the pinhole camera. An illustration of the geometry of the pinhole camera model is shown in Figure 3.2. From the two similar triangles appearing in Figure 3.2(b), we can derive the following equation

according to the similar-triangle principle:

$$\frac{-y_1}{f} = \frac{x_1}{x_3}. \tag{3.1}$$

When we look in the negative direction of the X_1-axis, the following equation can be derived similarly:

$$\frac{-y_2}{f} = \frac{x_2}{x_3}. \tag{3.2}$$

Summarizing these two equations, we get the following vector equation:

$$\begin{pmatrix} y_1 \\ y_2 \end{pmatrix} = -\frac{f}{x_3}\begin{pmatrix} x_1 \\ x_2 \end{pmatrix} \tag{3.3}$$

which describes the relation between the space coordinates (x_1, x_2, x_3) of a 3D point P and the image coordinates (y_1, y_2) of the 2D projection point Q.

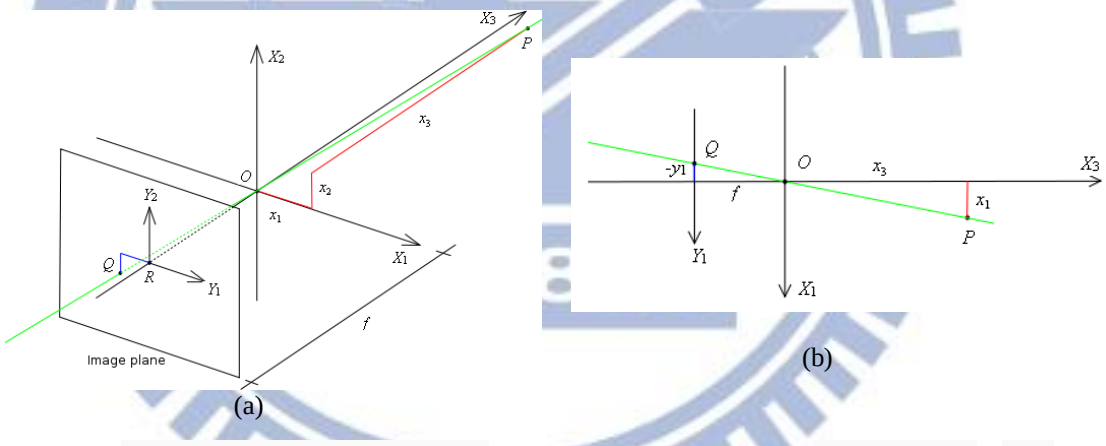

Figure 3.2 The geometry of a pinhole camera. (a) Seen from a 3D point. (b) Seen from the X_1-axis.

3.2 Construction of 3D Images

3.2.1 Coordinate Conversion

From Equation 3.3, we can get:

$$x_1 = -\frac{x_3}{f} \times y_1; \tag{3.4}$$

$$x_2 = -\frac{x_3}{f} \times y_2; \tag{3.5}$$

$$x_3 = \frac{x_3}{f} \times f\ . \tag{3.6}$$

And from Figure 3.2(a) and using the similar-triangle principle again, we have the equation:

$$\frac{x_3}{f} = \frac{\sqrt{x_1^{\,2} + x_2^{\,2} + x_3^{\,2}}}{\sqrt{(-y_1)^2 + (-y_2)^2 + f^2}} \tag{3.7}$$

where $\sqrt{(-y_1)^2 + (-y_2)^2 + f^2}$ is the length of the line segment *OQ*, and $\sqrt{x_1^{\,2} + x_2^{\,2} + x_3^{\,2}}$ is the length of the line segment *OP* which is the depth captured by KINECT device, and is denoted as *d* in the sequel. Let *R* present the center of the depth image. It is located at coordinates (320, 240) in a depth image of resolution 640×480 acquired by the KINECT device. And let *Q* be located at image coordinates (x_p, y_p) and let y_1 and y_2 represent the distances to the center *Q* in the vertical and horizontal directions, respectively. The letter *f* denotes the focal length of the KINECT device with its value being 600. The equations (3.7), (3.4), (3.5), and (3.6) can be rewritten, according to the mentioned parameter values, to be:

$$\frac{x_3}{f} = \frac{d}{\sqrt{(x_p - 320)^2 + (y_p - 240)^2 + 600^2}}; \tag{3.8}$$

$$x_1 = \frac{d}{\sqrt{(x_p - 320)^2 + (y_p - 240)^2 + 600^2}} \times (x_p - 320); \tag{3.9}$$

$$x_2 = \frac{d}{\sqrt{(x_p - 320)^2 + (y_p - 240)^2 + 600^2}} \times (y_p - 240); \tag{3.10}$$

$$x_3 = \frac{d}{\sqrt{(x_p - 320)^2 + (y_p - 240)^2 + 600^2}} \times 600. \quad (3.11)$$

The unit of x_p and y_p is pixel and that of x_1, x_2, and x_3 is millimeter. With the above equations, the coordinates in different coordinate systems can be converted successfully for 3D image construction as described next.

3.2.2 Idea of 3D Image Construction

The basic idea proposed in this study of 3D image construction is to convert the coordinates of the depth image described in Section 3.2.1 into 3D points. Then, we can draw these 3D points in the 3D space by the OpenGL. Finally, every RGB value of the pixel in the color image is "attached" to the corresponding 3D point. Colorful point clouds will be then formed in the resulting 3D image.

3.2.3 Construction Algorithm

In the proposed 3D image construction algorithm, assume first that the depth image coordinates are already converted into 3D points by coordinate conversion as described in Section 3.2.1. Then, it is desired to find the color information corresponding to each 3D point. By Equation (3.3) and the definitions given in Section 3.2.1, we have:

$$(x_p - 320) = -x_1 \times \frac{600}{x_3} \quad \text{or} \quad x_p = -x_1 \times \frac{600}{x_3} + 320; \quad (3.12)$$

$$(y_p - 240) = -x_2 \times \frac{600}{x_3} \quad \text{or} \quad y_p = -x_2 \times \frac{600}{x_3} + 240. \quad (3.13)$$

Therefore, the space coordinates (x_1, x_2, x_3) of a 3D point can be used to find the coordinates (x_p, y_p) of the corresponding image point. A flowchart of the resulting 3D image construction algorithm is shown in Figure 3.3. A detailed description of the

algorithm is as follows.

Algorithm 3.1: 3D image construction.

Input: a depth image I_d and a color image I_c captured by a KINECT device.

Output: a 3D image I_{3D} formed from I_d and I_c with colorful 3D points.

Steps:

Step 1 Convert the coordinates of the depth image I_d into 3D points by coordinate conversion described in Section 3.2.1.

Step 2 Substitute the coordinates of each 3D point into Equations (3.12) and (3.13) respectively to find the image pixel corresponding to the 3D point and get the pixel's color.

Step 3 Draw the 3D points in the 3D space with the corresponding colors by the OpenGL.

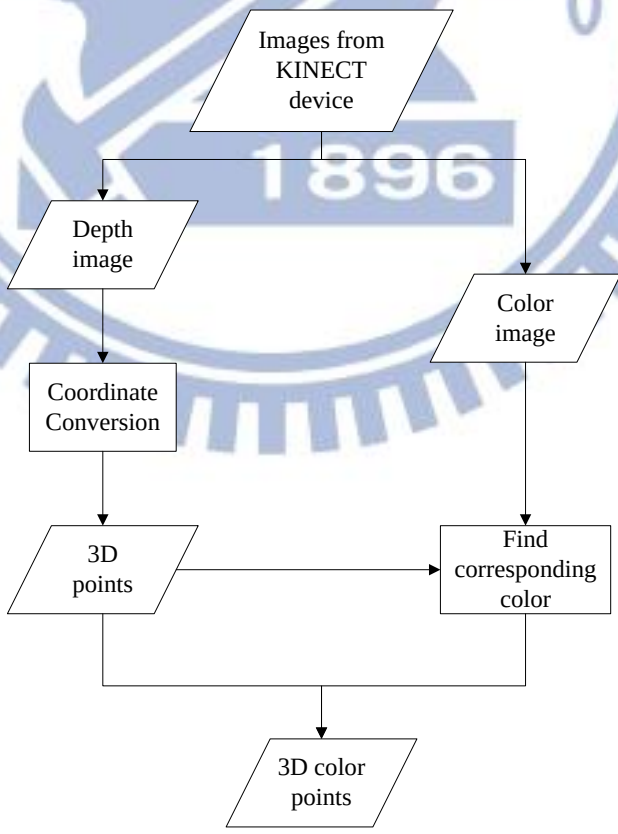

Figure 3.3 A flowchart of the 3D image construction algorithm.

3.2.4 Experimental Results

Figure 3.4 shows the depth image and the color image which are the inputs to the algorithm of 3D image construction. After the algorithm is executed, we have the 3D images, as shown in Figure 3.5. To prove the output of the algorithm to be three-dimensional, Figure 3.5 (b) shows the top view of the 3D image from which the depth of the car in the 3D image can be seen obviously, confirming the 3D nature of the output of the algorithm.

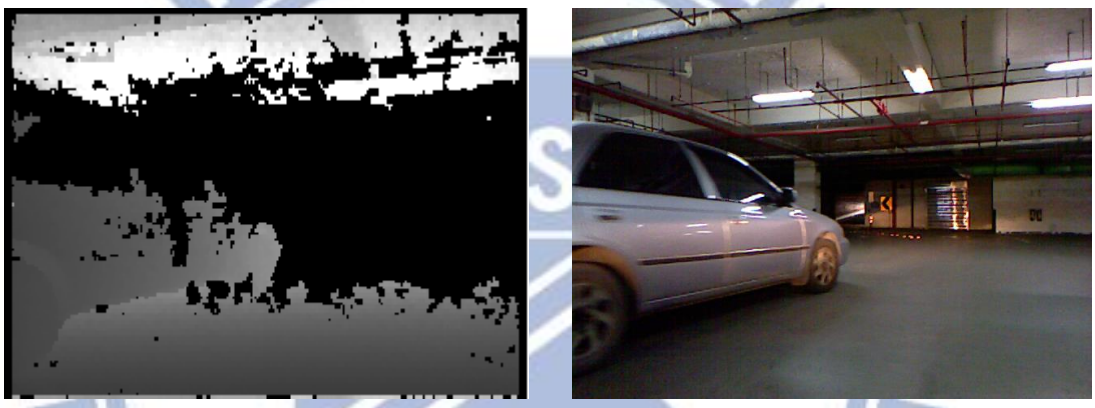

(a) (b)

Figure 3.4 Images acquired by a KINECT device. (a) The depth image. (b) The color image.

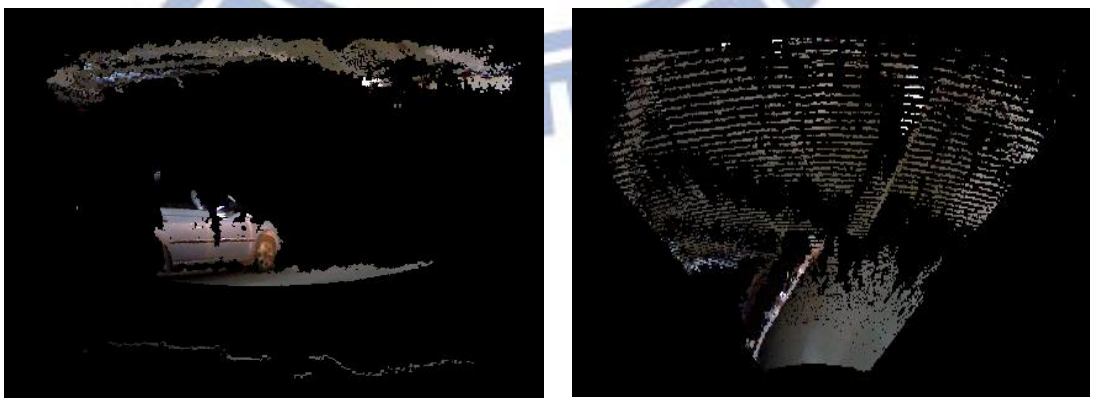

(a) (b)

Figure 3.5 A constructed 3D image. (a) A perspective view. (b) A top view.

3.3 Review of a method for Geometric Correction of 3D Images

3.3.1 Idea of Geometric Correction

From Figure 3.5 (b) in Section 3.2.4, we discovered that the farthest points of the depth image form an arc shape rather than a straight line. The reason why this problem arises is that the infrared light rays sent out by the KINECT device for depth sensing do not go in parallel as mentioned in Section.1.3. It affects the accuracy of the depth because the depth is not the vertical distance anymore. In order to solve the problem, a method for geometric correction of 3D images [9] is adopted.

The idea behind the proposed geometric correction method is that we use a paraboloid to approximate the curved surface formed by the farthest points of the depth image mentioned previously. Once the approximating paraboloid is found, the values of the coordinates *x* and *y* of each space point are substituted into the equation of the paraboloid to correct the computed distance, as shown in Figure 3.6.

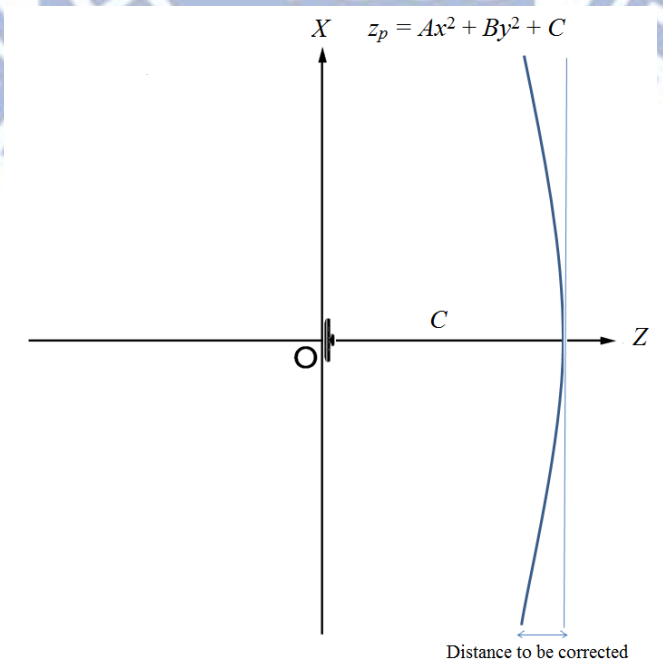

Figure 3.6 The paraboloid seen from the direction of the *Y*-axis (from the top view).

3.3.2 Correction Algorithm and Experimental Results

In this section, the method for finding the approximating paraboloid is described and some experimental results are shown. The criterion of minimum sum of squared errors (MSSE) is used to decide the parameters of the approximating shape which is a paraboloid. The following is the detail of this process.

First, let the equation of the paraboloid be described by:

$$z_p = A \times x^2 + B \times y^2 + C \tag{3.14}$$

where C is the distance between the KINECT device and the apex of the paraboloid, as shown in Figure 3.6. The equation for computing the value *SSE* of the SSE is:

$$SSE = \sum_{i=0}^{i=640\times480} \left[z_i - \left(A \times x_i^{\,2} + B \times y_i^{\,2} + C \right) \right]^2 \tag{3.15}$$

where (x_i, y_i, z_i) are the coordinates of a sample point. To find the coefficients A, B and C which minimize the SSE value, we compute the partial derivatives of Equation (3.15) with respect to variables A, B and C, respectively, leading the following equations:

$$-2 \times \sum_{i=0}^{i=640\times480} \left[z_i - \left(A \times x_i^{\,2} + B \times y_i^{\,2} + C \right) \right] \times \left(-x_i^{\,2} \right) = 0; \tag{3.16}$$

$$-2 \times \sum_{i=0}^{i=640\times480} \left[z_i - \left(A \times x_i^{\,2} + B \times y_i^{\,2} + C \right) \right] \times \left(-y_i^{\,2} \right) = 0; \tag{3.17}$$

$$-2 \times \sum_{i=0}^{i=640\times480} \left[z_i - \left(A \times x_i^{\,2} + B \times y_i^{\,2} + C \right) \right] \times 1 = 0. \tag{3.18}$$

The values of A, B and C are computed by solving the simultaneous equations (3.16), (3.17) and (3.18). Since we have all the values of x_i, y_i and z_i, the equations (3.16), (3.17) and (3.18) become the three-variable linear equations after substituting all the values of x_i, y_i and z_i into the simultaneous equations. By solving these three independent equations, the values of A, B and C can be computed analytically. The

demanded paraboloid is so obtained. Finally, we show some examples of the experimental results in Figures 3.7 and 3.8.

(a) (b)

Figure 3.7 A correction result of Figure 3.5 (b). (a) Before correction. (b) After correction.

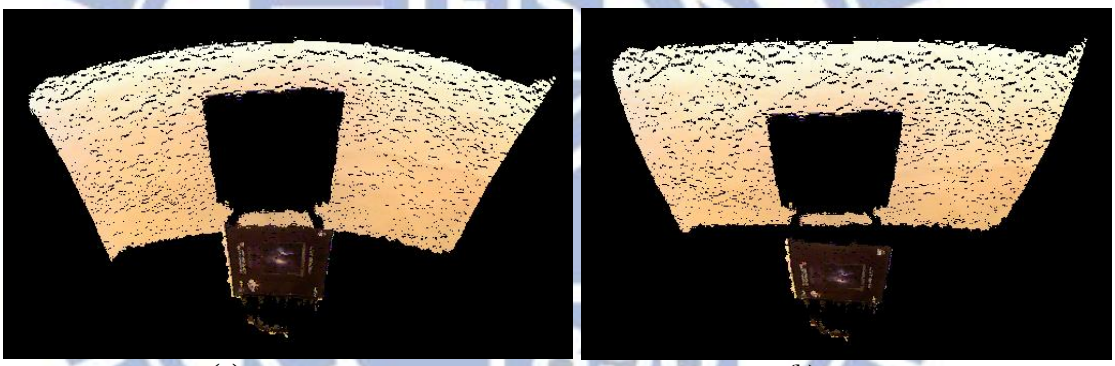

(a) (b)

Figure 3.8 A 3D image seen from above. (a) Before correction. (b) After correction.

Chapter 4
Modeling of Around-car Events

4.1 Construction of Around-car 3D Images

In this chapter, we describe the method we propose for modeling of around-car events. In Section 4.1.1, the iterative closest point (ICP) algorithm and the K-D tree algorithm [10] used in this study are reviewed. In Section 4.1.2, how the calibration work is done by using the ICP algorithm to find the geometric relationship between every two KINECT devices is presented. With the calibration information, the idea and algorithm for constructing the around-car model are proposed in Sections 4.1.3 and 4.1.4, respectively. Finally, we show some experimental results in Section 4.1.5.

4.1.1 Review of Iterative Closest Point (ICP) Algorithm and K-D Tree Algorithm

The iterative closest point (ICP) algorithm can be employed to minimize the difference between two groups of points. The concept of the algorithm is simple. It revises the transformation, including rotation and translation, from one object to the other, iteratively in order to minimize the *total distance* measure between the two groups of points.

The ICP is often used to match objects to compute their similarity. It is found useful for constructing 2D or 3D images from different views because object

registration or stitching, which is needed in this study, requires shape matching before the work is conducted.

A K-D tree algorithm is also employed in this study to reduce the amount of computation for searching the closest point using the ICP algorithm. The method for constructing a K-D tree, simply speaking, is to separate the group of points in concern into two parts by the median of the *X*, *Y* and *Z* coordinates sequentially. When searching the closest point, it takes less time to search a K-D tree rather than to search all the points. The complexity of searching becomes $O(N^{2/3})$ from $O(N)$.

4.1.2 Calibration between Neighboring KINECT Devices Using ICP

In Section 4.1.1, it was mentioned that the ICP algorithm can be employed to minimize the difference between two groups of points. This inspired us to get the idea that we might use the ICP algorithm to "register" two objects if the two groups of points composing the objects are similar in their features. So, a method of calibration of the geometric relationship between two neighboring KINECT devices using the ICP algorithm is proposed in this study, and is described in this section.

First, a carton is put between every two neighboring KINECT devices as the calibration target. Then, depth images are acquired with these two KINECT devices, respectively. At this moment, we have two similar groups of points which come from an identical object, the carton, but appear in two different views. After the ICP algorithm is applied to register them, geometric relationship parameters, including the horizontal included angle and the displacements along the *x*-, *y*- and z-axes can be obtained. This completes the calibration of the geometric relationship between two neighboring KINECT devices. A detailed description of this process as an algorithm is

as follows.

Algorithm 4.1: calibration between two neighboring KINECT devices using the ICP algorithm.

Input: depth images I_1 and I_2 of a calibration target (a carton) acquired respectively with two neighboring KINECT devices D_1 and D_2.

Output: the geometric relationship parameters, a horizontal included angle θ_i and a 3D displacement d_i, of D_1 and D_2.

Steps:

Step 1 Convert the coordinates of the depth images I_1 and I_2 into two groups G_1 and G_2 of 3D points, respectively, by the coordinate conversion scheme described in Section 3.2.1.

Step 2 Move group G_1 of 3D points iteratively through a series of transformations T_i, each including a horizontal included angle θ_i and a 3D displacement $d_i = (d_{ix}, d_{iy}, d_{iz})$ along the *x*-, *y*- and z-axes, respectively.

Step 3 For each transformation $T_i = (\theta_i, d_i)$, compute the Euclidean distances D_{jk} from each point P_j of G_1 to every point P_k of G_2.

Step 4 For each point P_j, choose the minimum distance D_{jm} from the distances D_{jk}.

Step 5 Sum up all the D_{jm} as the distance D_i for T_i between G_1 and G_2.

Step 6 Find the transformation $T_i = (\theta_i, d_i)$ with the minimum D_i as the desired relationship parameters.

4.1.3 Idea of Proposed Method for Around-car Scene Model Construction

According to the discussions in Section 3.2, we can construct a 3D partial scene model by the use of a single KINECT device. To construct the around-car 3D scene

model, a technique to use of multiple KINECT devices simultaneously is needed. And the relationship information for every two KINECT devices, which is obtained during calibration as described previously, is also needed. Under these conditions, we can start to construct the around-car scene model.

4.1.4 Construction Algorithm

In Section 2.1, we discuss how to use a desktop computer to control multiple KINECT devices to work simultaneously via a USB expansion card. As for calibration, the proposed method for acquiring the geometric relationship parameters between neighboring KINECT devices has been described in Section 4.1.2. A flowchart of the proposed around-car model construction algorithm is shown in Figure 4.1. And a detailed description of the algorithm is as follows.

Algorithm 4.2: around-car scene model construction.

Input: images I_1 through I_{14} acquired with the 14 around-car KINECT devices, respectively.

Output: an around-car model M_{car}.

Steps:

Step 1 Construct 3D models M_1 through M_{14} using images I_1 through I_{14}, respectively, by the 3D image construction scheme described in Section 3.2.3.

Step 2 For i = 1~13, compute the geometric relationship parameters R_i between the 3D models M_i and M_{i+1} iteratively by the calibration algorithm (Algorithm 4.1) described in Section 4.1.2, with each R_i including a horizontal angle θ_i and a 3D displacement d_i = (d_{ix}, d_{iy}, d_{iz}) along the x-, y- and z-axes, respectively.

Step 3 For i = 1~13, perform the following steps.

3.1 Rotate the *x*- and z-axes of 3D model M_{i+1} by horizontal angles θ_1 through θ_i iteratively in order to match the coordinate system of 3D model M_1.

3.2 Move the coordinates of 3D model M_{i+1} through a series of 3D displacements, namely, d_1, d_2, …, d_i iteratively to form an around-car model M_{car}.

Step 4 Display an around-car model M_{car} by drawing all the point sets P_1 to P_{14} of 3D models M_1 to M_{14}, respectively, in the 3D space with the OpenGL.

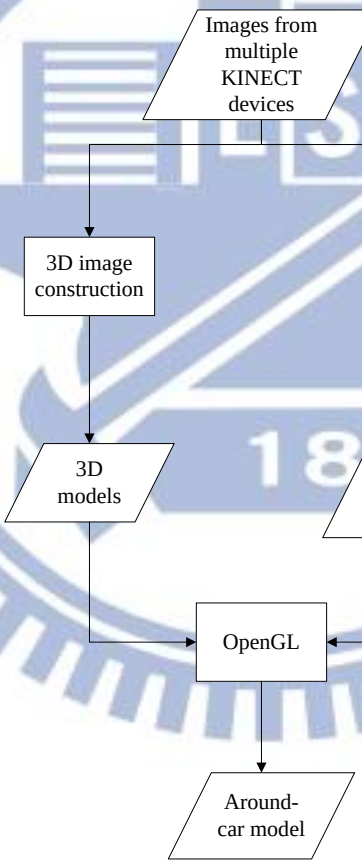

Figure 4.1 A flowchart of the around-car model construction algorithm.

4.1.5 Experimental Results

In this section, some experimental results of conducting Algorithm 4.2 for

around-car scene model construction are shown. At first, the comparative illustrations from Section 4.1.2 are shown in Figure 4.2. From Figure 4.2(b), it can be seen that after calibration, the 3D models of the identical cartons constructed from images acquired with two neighboring KINECT devices overlap each other well. Then, the constructed around-car model is shown from each of the three sides of the car respectively, as shown in Figure 4.3.

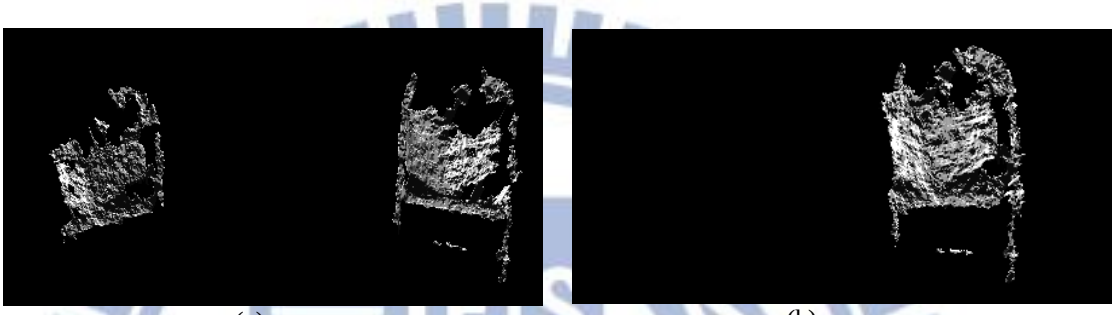

(a) (b)

Figure 4.2 Comparison of constructed 3D scene models before and after calibration. (a) Before calibration. (b) After calibration.

(a)

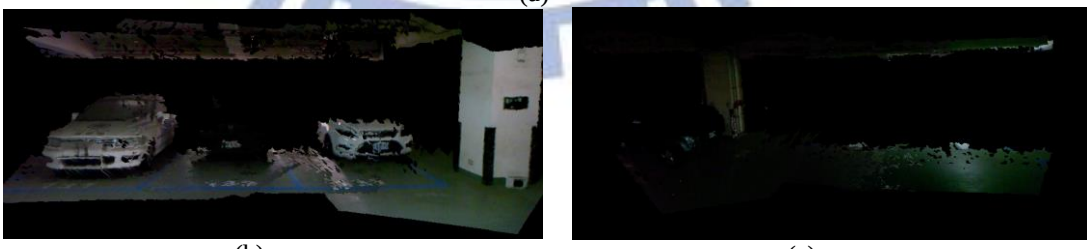

(b) (c)

Figure 4.3 The constructed around-car model. (a) Front view. (b) Left side view. (c) Right side view.

4.2 Modeling of a By-passing Car Using 3D Distance-weighted Correlation (DWC)

4.2.1 Review of DWC

The measure of distance-weighted correlation (DWC) was proposed by Fan and Tsai [11] originally for automatic Chinese seal identification. The measure is defined as the minimum distance between two groups S and T of pixels of seal imprint images after the seal imprint images are overlapped. For each pixel p in S, a pixel in T with the minimum distance to p is searched for. If the result is a pixel p' within a limited circular area A with a pre-selected radius K, then a weight $w_p^K = 1/(d_p^2 + 1)$ is defined where d_p is the distance from p to p'; otherwise, the weight w_p^K is defined to be zero. That is, for each pixel p in S, a weight w_p^K is defined as follows:

$$\begin{aligned} w_p^K &= \frac{1}{d_p^2+1}, && \text{if } 0 \le d_p \le K, \\ w_p^K &= 0 && \text{otherwise,} \end{aligned} \tag{4.1}$$

where d_p is the distance of p in S to the closest point p' in T. Note that K is a threshold used to decide an *effective* distance; distances larger than this threshold is discarded. Finally, the DWC defined for the two groups of pixels, S and T, is defined as follows:

$$C^K(S,T) = \frac{1}{2} \times \left(\frac{1}{N_S} \sum_{s \in S} w_s^K + \frac{1}{N_T} \sum_{t \in T} w_t^K \right), \tag{4.2}$$

where the coefficient 1/2 is included to treat S and T symmetrically; and N_S and N_T are the total numbers of pixels in S and T, respectively. It can be verified that $0 \le C^K \le 1$ and $C^K = 1$ if and only if $S = T$. The DWC, though defined originally for seal

identification, is a general measure for *point-type* object shape matching.

4.2.2 Proposed 3D DWC

An extension of the above-reviewed "2D" DWC measure is proposed in this study for the purpose of 3D scene model construction. However, the 2D DWC was used to decide whether the images of two object shapes are similar or not, while the proposed 3D DWC is used to compute the displacement of two similar objects in this study.

4.2.3 Idea of Modeling of a By-passing Car Using 3D DWC

The depth range of the KINECT device is limited and the horizontal angle is only 57 degrees, so we cannot acquire the 3D information of the entire scene from a single image frame. Therefore, it is difficult to construct a complete model of a scene with only one KINECT device, or equivalently, with only a pair of color and depth images acquired with a single KINECT device. But we discovered that the models in any two sequential image frames acquired with two neighboring KINECT devices, when acquired with a high frame rate, are very similar. Since it is possible to overlap the two similar objects by the 3D DWC as mentioned previously, the 3D DWC can thus help us construct the model of a scene from different frames acquired with distinct KINECT devices. As the 3D information increases, it is possible to construct a more complete model of a scene.

4.2.4 Modeling Algorithm

In the proposed scene modeling algorithm, it is assumed first that a 3D model is

already constructed by one KINECT device as described in Section 3.2. Then, by the use of the 3D DWC, we compute the displacement between the 3D models which are constructed from the images acquired with every two KINECT devices. By using all the resulting displacements, it is feasible to construct a more complete model of a scene. In this study, the mainly concerned object in the scene model is a by-passing car. A flowchart of the modeling algorithm is shown in Figure 4.4. A detailed description of the algorithm is as follows.

Algorithm 4.3: modeling of a by-passing car using 3D DWC.

Input: a series I of image pairs $I_1, I_2, \ldots, I_n$ acquired of a by-passing car M_{car} with n KINECT devices, with each image pair I_i including a color image I_{ci} and a depth image I_{di}.

Output: a 3D model of M_{car}.

Steps:

Step 1 Assuming that the car is driven in a road lane, learn the threshold T of the width of the lane in the depth images beforehand in order to remove background image parts beyond the lane in the next step.

Step 2 Perform the following steps to filter out unrelated scene parts other than the car in each image pair I_j, respectively, by the thresholds T learned in Step. 1:

2.1 for each pixel p in the depth image I_{dj}, if the depth value of p is larger than T, then remove p from I_{dj};

2.2 for each pixel p' in the color image I_{cj}, if the corresponding pixel p in I_{dj} is removed, then also remove p' from I_{cj}.

Step 3 For each image pair I_j, construct a 3D model of the by-passing car M_j by the 3D image construction scheme described in Section 3.2.3.

Step 4 For $j = 1$ through $n - 1$ (i.e., for every two neighboring car models), perform the following steps to construct a complete car model M_{car}:

4.1 compute the 3D displacement $d_j = (d_{jx}, d_{jy}, d_{jz})$ along the x-, y- and z-axes, respectively, by matching the two partial car models M_j and M_{j+1} by the use of the 3D DWC measure described previously.

4.2 overlap the two partial car models M_j and M_{j+1} in accordance with the computed 3D displacements d_j to form a new model to replace the original partial model M_{j+1}.

Step 5 Display the resulting car model M_{car} of the last step by drawing all the overlapped points of M_{car} in the 3D space with the OpenGL.

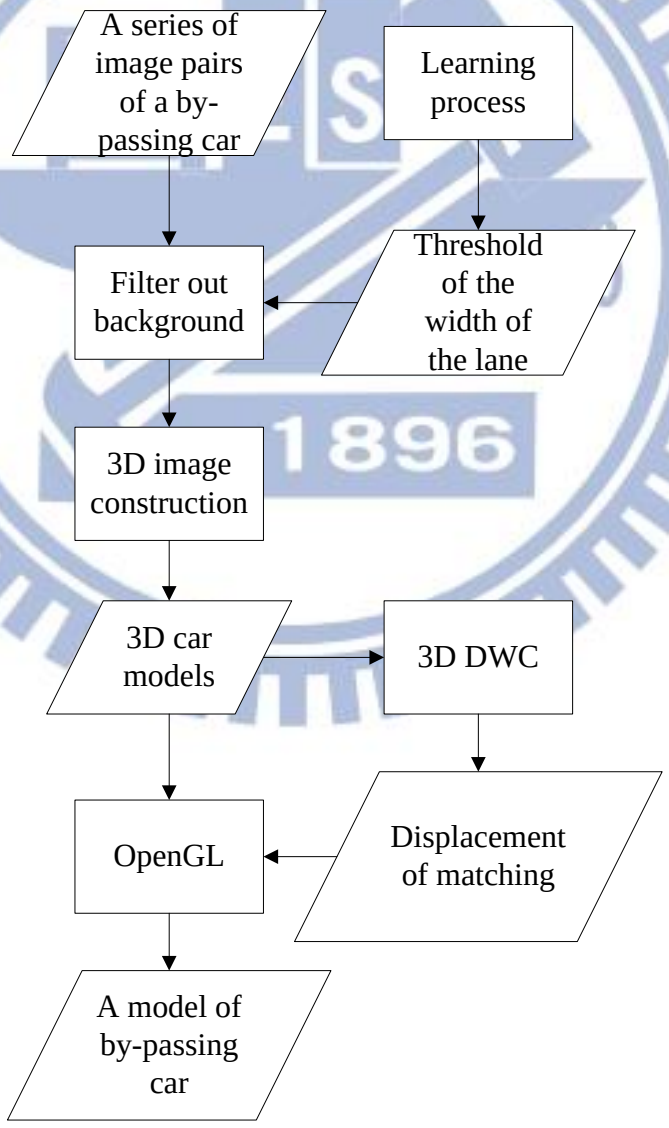

Figure 4.4 A flowchart of the car modeling algorithm.

4.2.5 Experimental Results

In this section, an example of the 3D models of the by-passing car resulting from executing Algorithm 4.3 described previously is shown in Figure 4.5. It is obvious that with more image frames, the constructed model of the by-passing car becomes more complete. Furthermore, from Figure 4.5(a) we can see only the middle part of the car, but from Figure 4.5(d) we can see its rear part. This experimental result shows the effectiveness of the use of the 3D DWC measure for 3D object modeling.

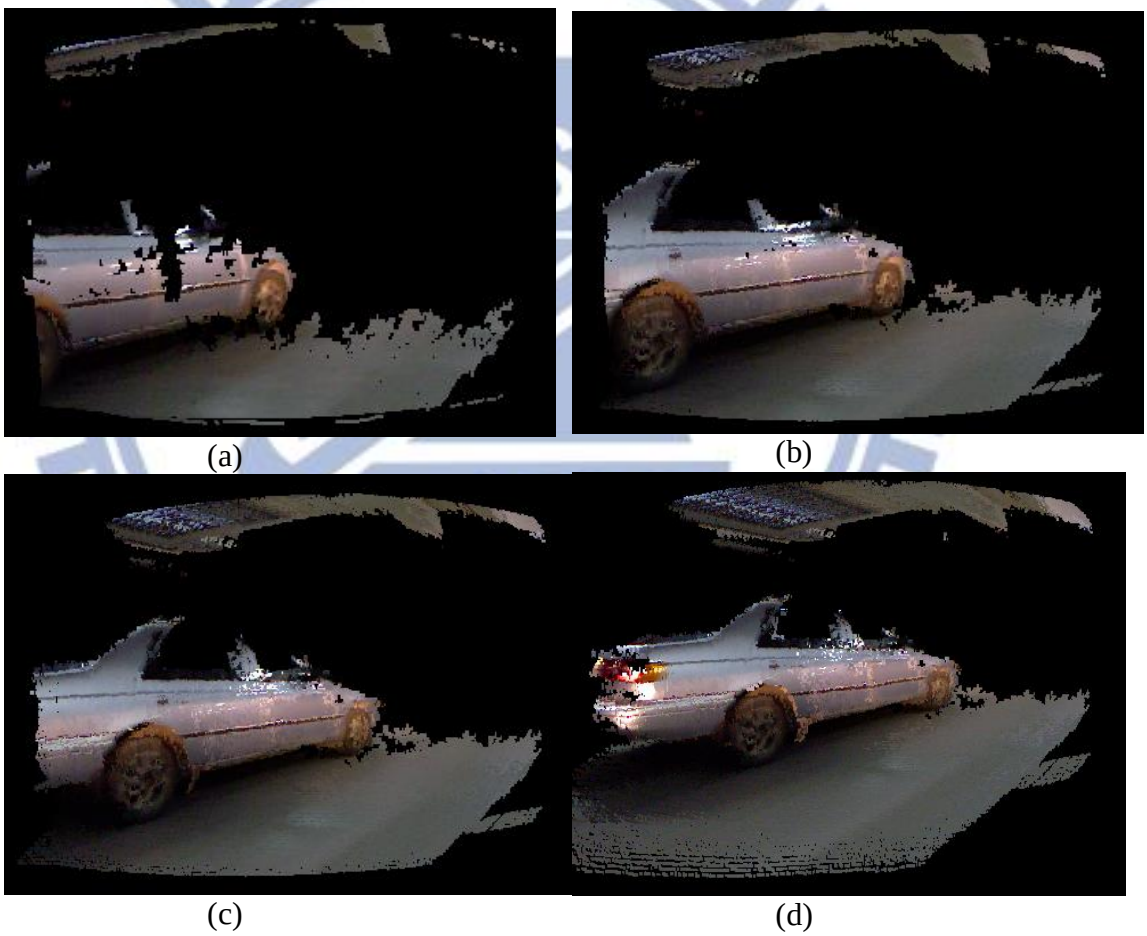

Figure 4.5 The models of a by-passing car constructed by overlapping different numbers of frames. (a) By one frame. (b) By five frames.(c) By ten frames. (d) By fifteen frames.

4.3 Restoration of Car-accident Scenes

4.3.1 Idea of Restoring Car-accident Scenes Using 3D DWC

Since the depth range yielded by the KINECT device is limited, as described previously, once the distance between the KINECT device and the object is out of the range, it becomes impossible to acquire the depth information. In addition, when a car accident occurs, we need to construct the models of the involved cars in order to clarify the responsibility of the car accident by inspecting the relative geometric conditions of the constructed car models. But the distance between the cars in a car accident is usually smaller than the minimum value of the depth range. Nevertheless, from the Section 4.2, we know that it is possible to increase 3D information by overlapping the models in continuous frames. That is, we can construct a more complete model of the involved car in the car accident by overlapping the models in the previous frames. This means that we can use the 3D DWC measure to restore a car accident scene. More details are presented in the following.

4.3.2 Restoring Algorithm

First, the depth and color images of the involved cars which appear just before the car collision happens are needed. Then, the backgrounds and the depth information, which do not belong to the car, are filtered out to construct the car models more easily. Next, the displacement for overlapping the car models is computed by the use of the 3D DWC measure, as done previously. Once the models of the involved cars are overlapped accurately with the displacement, we can restore the car accident scene by constructing more complete models of the involved cars. A

flowchart of the restoration algorithm is shown in Figure 4.6. A detailed description of the algorithm is as follows.

Algorithm 4.4: restoring of a car-accident scene using 3D DWC.

Input: an image sequence I_1 through I_n of an involved car (other than the one on which the proposed system is installed) in a car-accident.

Output: a complete model M_{car} of the involved car.

Steps:

Step 1 Pick out the image I_j of the involved car which appears just before the car collision occurs by inspecting the image sequence I_1 through I_n acquired of the involved car.

Step 2 Construct 3D models M_1 through M_j from images I_1 through I_j by the 3D image construction scheme described in Section 3.2.3.

Step 3 For k = 1, 2, …, j–1, compute the 3D displacement $d_k = (d_{kx}, d_{ky}, d_{kz})$ along the x-, y- and z-axes, respectively by matching the car models M_k and M_{k+1} by the use of the 3D DWC scheme mentioned in Section 4.2.2.

Step 4 For k = 1, 2, …, j–1, overlap the car models M_k and M_{k+1} in accordance with the computed 3D displacements d_k to form a more complete model of the involved car M_{car}.

Step 5 Display M_{car} by drawing all the points in M_{car} in the 3D space with the OpenGL.

4.4 Experimental Results

Due to security concerns, a toy car was used to simulate car accidents in this experiment. Figure 4.7 shows the models of the car before the instant of collision in a simulated car accident in different frames, respectively. The green lines simulate the

range of our car on which the proposed system is installed. In Figure 4.7(d), we can see that part of the toy car passes through the area surrounded by the green lines. It means that the toy car collides with our car. By the constructed model, it is feasible to restore a car-accident scene and check the responsibility in law.

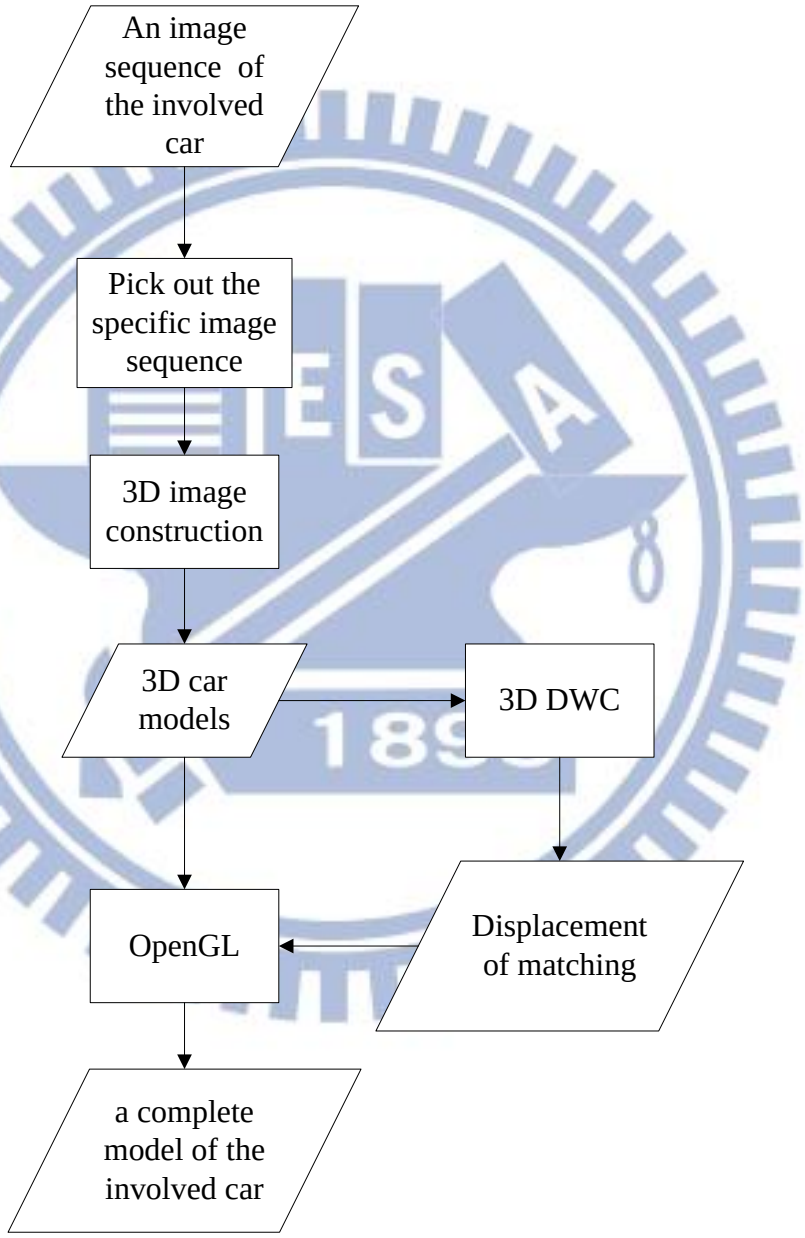

Figure 4.6 A flowchart of the restoring algorithm.

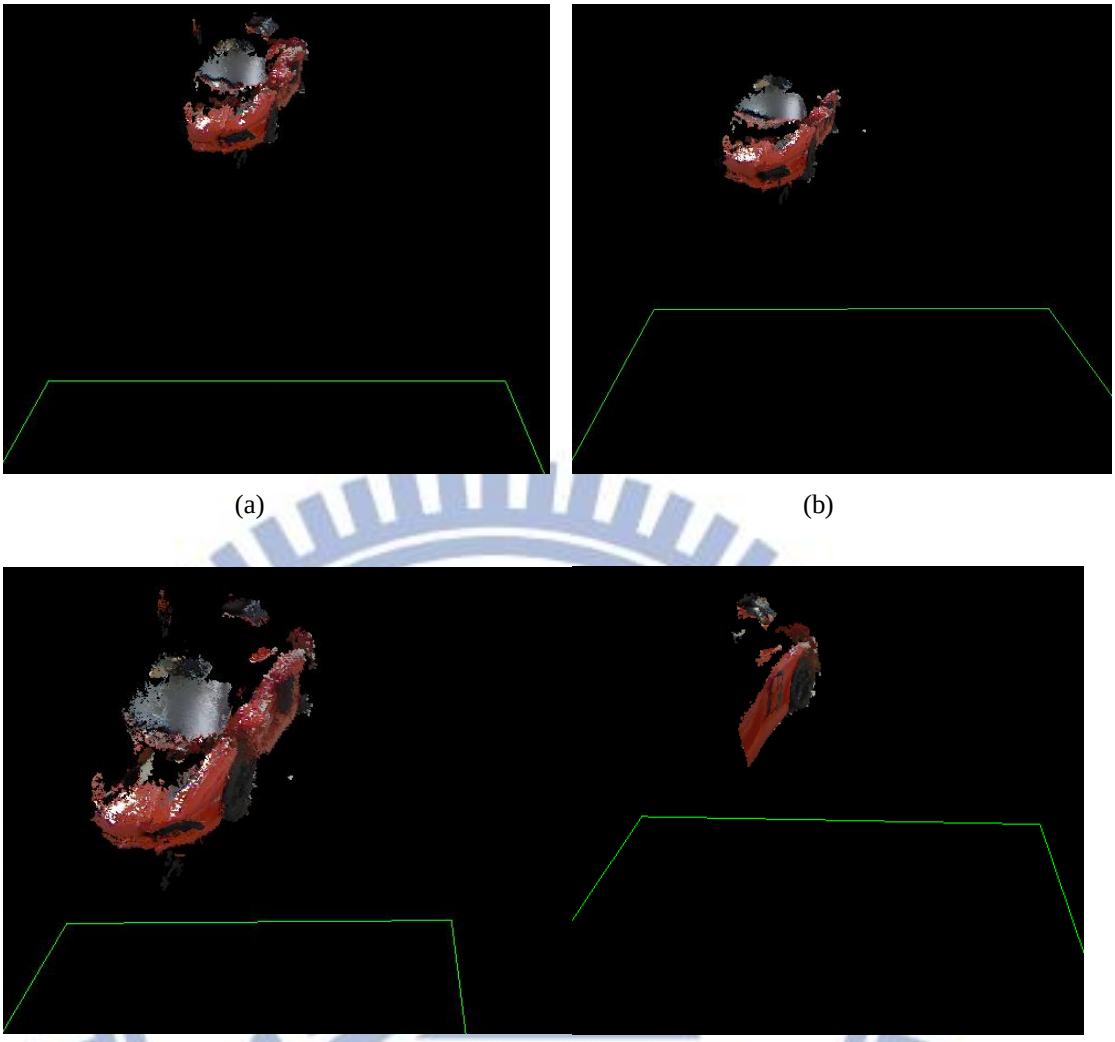

(a) (b)

(c) (d)

Figure 4.7 Models of an involved car before the instant of collision in different frames. (a) 60 frames before. (b) 40 frames before. (c) 20 frames before. (d) At instant of collision.

Chapter 5
Real-time Response to Around-Car Dangerous Events

5.1 Monitoring of Ramps on Roads

5.1.1 Idea of Monitoring of Ramps on Roads

The slope of the ramp, especially that of a downhill one, is important information for a driver while driving on the road. The speed of the car will rise because of the gravity when driving on a downhill road. As the speed of the car goes up, it reduces the driver's reaction time. That will be a potential danger to driving safety. In order to reduce the danger, we propose a method of using KINECT images and trigonometric functions and mathematical geometry to measure the slope of the ramp. In this way, the driver can know the slope of the ramp before driving downhill. If the driver is able to slow down earlier on a steep downhill road, the driving safety is improved.

5.1.2 Monitoring Algorithm and Experimental Results

In the proposed method, the KINECT device we use is mainly the one affixed in the front of the car, which is tilted down thirty degrees in order to increase the acquired depth information of the road, as shown in Figure 5.1. As seen in Figure 5.2, let θ_3 represent the slope of the ramp. Then, it can be easily figured out from

trigonometry that

$$\theta_3 = \theta_1 - \theta_2 \tag{5.1}$$

where θ_1 is 30^o as mentioned previously, and according to trigonometry again, we have:

$$\theta_2 = \tan^{-1}(\frac{\Delta Y}{\Delta Z}) \tag{5.2}$$

where ΔY and ΔZ can be computed by points $P(Y_1, Z_1)$ and $Q(Y_2, Z_2)$ which are selected from the centerline of the KINECT device on the ramp. By Equation 5.1, the slope of the ramp θ_3 can be computed. A flowchart of the algorithm is shown in Figure 5.3. A detailed description of the algorithm for this process is as follows.

Algorithm 5.1: computing the slope of a ramp.

Input: a depth image *I* acquired with the KINECT device affixed in the front of the car.

Output: a slope of a ramp.

Steps:

Step 1 Select the lowest pixel point *P* on the image boundary from the centerline of the depth image *I*.

Step 2 Select the center point *Q* of the depth image *I*.

Step 3 Convert the coordinates and the depth values of pixel points *P* and *Q* into 3D points $P(X_1, Y_1, Z_1)$ and $Q(X_2, Y_2, Z_2)$, respectively, by the coordinate conversion scheme described in Section 3.2.1.

Step 4 Compute ΔY and ΔZ by subtracting the values of Y_1 and Z_1 of point *P* from the values of Y_2 and Z_2 of point *Q*, respectively, i.e., compute $\Delta Y = Y_1 - Y_2$ and $\Delta Z = Z_1 - Z_2$.

Step 5 Compute the angle θ_2 by Equation 5.2.

Step 6 Compute as output the slope of the ramp θ_3 by Equation 5.1.

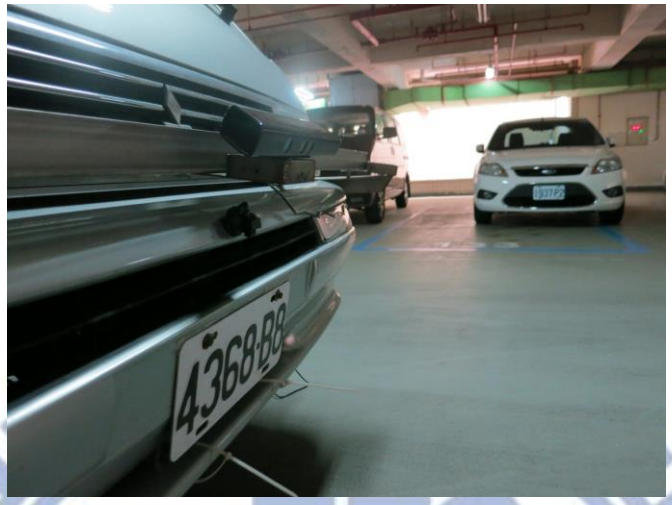

Figure 5.1 The KINECT device affixed in the front of the car and it is tilted down thirty degrees.

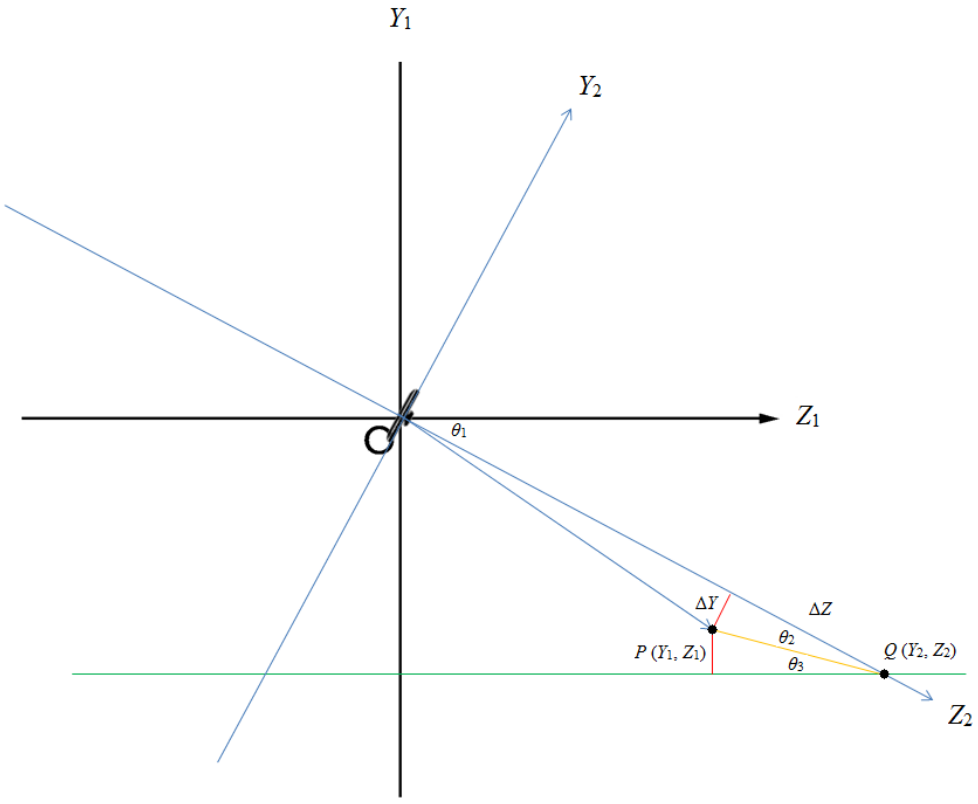

Figure 5.2 Geometry of slope computation where the orange-colored line represents a slope.

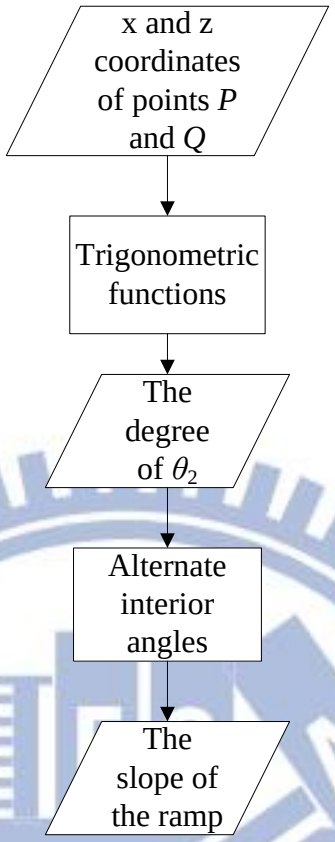

Figure 5.3 A flowchart of computing slopes algorithm.

Once the slope of the ramp θ_3 is computed, it is feasible to compute the magnitude of gravity *g*, as shown in Figure 5.4. From the figure, we have:

$$a = g \times \cos(90^{o} - \theta_3) \tag{5.3}$$

where *a* represents the acceleration of the car along the ramp. Some results of computations of the value *a* in different slopes are shown in Table 5.1. Assume that the ramp is 100m long and the car speed is 40 km/hr. It takes 9 seconds to pass the ramp without the acceleration *a*. Once we have the acceleration, the time is shorter than 9 seconds. By the constant acceleration equation, we have:

$$l = s \times t + \frac{1}{2} \times at^2 \tag{5.4}$$

where *t* denotes the passing time, *s* is the car speed, and *l* is the length the car goes. By

substituting the acceleration a = 17.64 km/hr, the car speed s = 40 km/hr, and the slope length l = 100m into Equation (5.4), we can get the solution, the passing time, to be about 4.5 seconds which is a half of 9 seconds. It means that if the slope of the ramp is more than 30 degrees, the time will be less than a half of the time required for normal driving on flat road surfaces. Therefore, the driver should slow down the car speed to avoid danger.

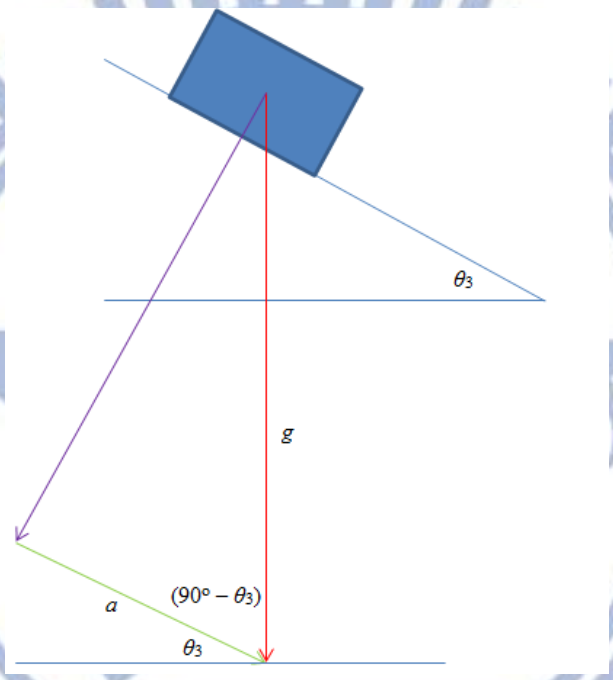

Figure 5.4 The components of gravity g.

Table 5.1 The results of computations in different slopes.

Slope θ_3	10^o	20^o	30^o	40^o	50^o	60^o
Acceleration a	6.12	12.06	17.64	22.68	27.03	30.55 km/hr

We now show some experimental results of applying the above algorithm to real situations. Figures 5.5 and 5.6 show two different results on the ground and on a ramp, respectively. Figures 5.5(a) and 5.6(a) show respective images of the ground and the

ramp in front of the car while Figures 5.5(b) and 5.6(b) respectively show the slopes of the ground and the ramp, respectively. The repeated values in Figures 5.5(b) and 5.6(b) denote keep monitoring the ramp.

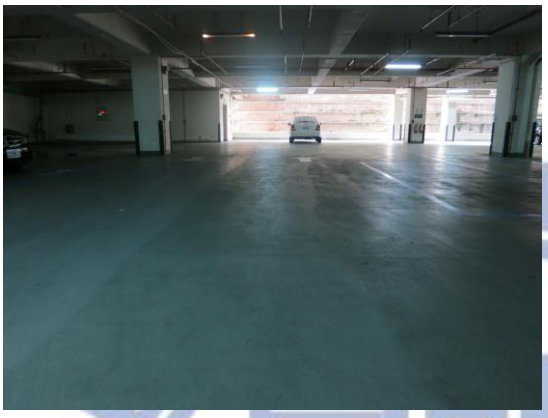

(a)

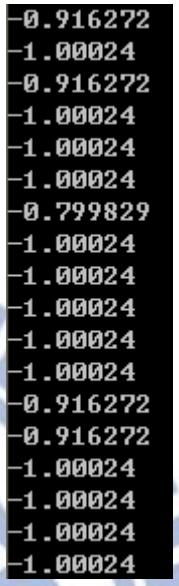

(b)

Figure 5.5 The experimental result on the ground. (a) Front view from the car. (b) The values of the slope.

(a)

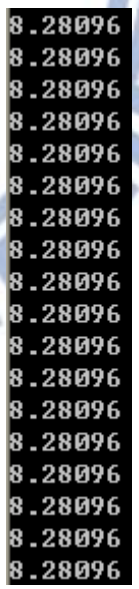

(b)

Figure 5.6 The experimental result on the ramp. (a) Front view from the car. (b) The values of the slope.

5.2 Monitoring of Limitations of Heights on Roads

5.2.1 Idea of Monitoring of Limitations of Heights on Roads

When driving on the road, there are some places where limitations on the car height are imposed, such as at the entrance of a parking lot, while going through a road under a bridge, etc. Despite of the fact that normally, there is a height limit sign which is used to warn the driver of hitting the car roof, the driver generally does not know the actual height of their car. Once the driver misjudges the height of the car, an accident of hitting the car roof might happen. To avoid such an accident, we use the KINECT device which is affixed on the front top of the car to monitor the height-restricting barriers and calculate the height difference between them.

5.2.2 Monitoring Algorithm and Experimental Results

As mentioned previously, the KINECT device affixed on the front top of the car as shown in Figure 5.7 is used to monitor height-restricting barriers and calculate the height difference between the car roof and the barriers. Now, we describe the proposed method to do so. From Figure 5.8, we see that y_1 of point P denotes the height of the car roof and y_2 of the point Q denotes the lowest height of the height-restricting barrier. Let Δy be the height difference between the points P and Q. We search for the point Q from the point P along the continuous depth points in the negative direction of the y-axis. The endpoint of the continuous depth points is the

point Q. The coordinates of points P and Q are then converted by coordinate conversion scheme mentioned in Section 3.2.1. With these steps, the difference between the car roof and the height-restricting barriers is acquired for security warning uses. A flowchart of computing the height difference is shown in Figure 5.8. A detailed description of the algorithm is as follows.

Algorithm 5.2: calculating the height difference between the car roof and the height restriction barriers.

Input: a depth images I_d from the KINECT device affixed on the front top of the car.

Output: the height difference between the car roof and the height-restricting barriers.

Steps:

Step 1 Find the center point P of the depth images I_d.

Step 2 Convert the coordinates of the depth image I_d into 3D points by the coordinate conversion scheme described in Section 3.2.1.

Step 3 Search the endpoint Q at the image boundary from the point P along the continuous depth points in the negative direction of the y-axis.

Step 4 Compute as output the height difference Δy by subtracting the value of y_1 of point P from the value of y_2 of point Q.

With the height difference Δy computed, we can use it to warn the driver of possible hitting on the car roof if Δy is approaching zero. The car will soon be hit on the roof when Δy becomes zero.

Some experimental results are shown in Figure 5.10. In the image of Figure 5.10(a), the relationship between the KINECT device affixed on the front top of the car and a height-restricting barrier can be seen. From Figure 5.10(b), the computed value of the height difference using the algorithm is shown.

Figure 5.7 The KINECT device affixed on the front top of the car.

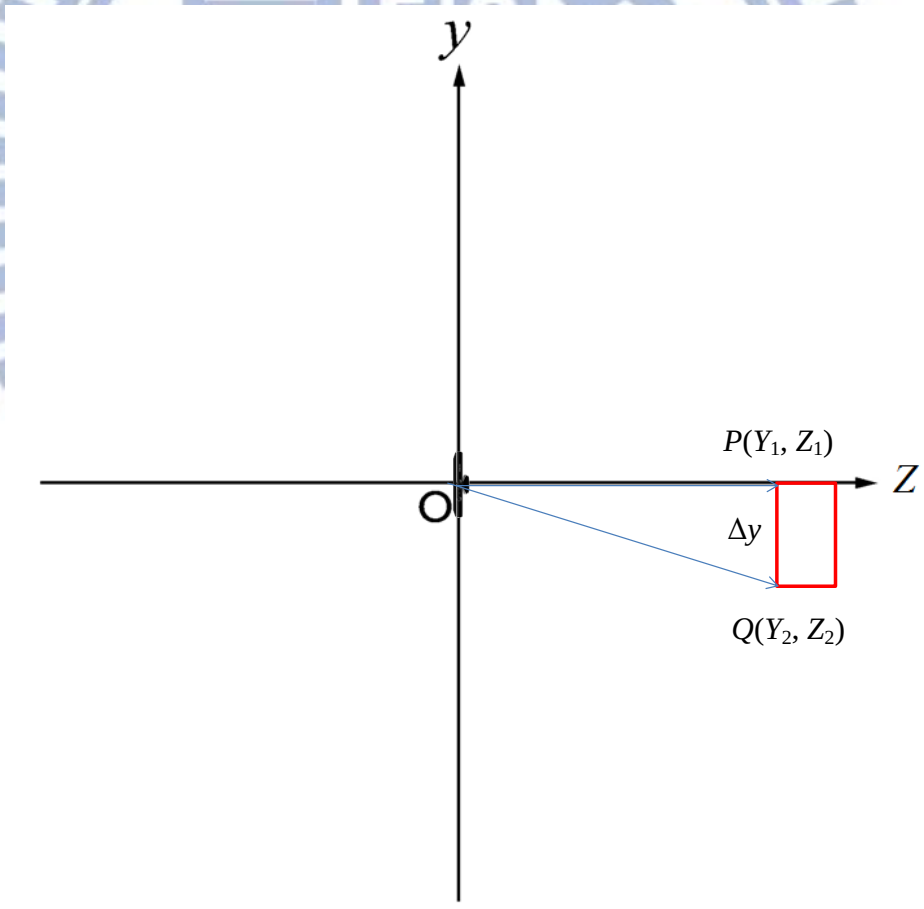

Figure 5.8 A computation of height difference.

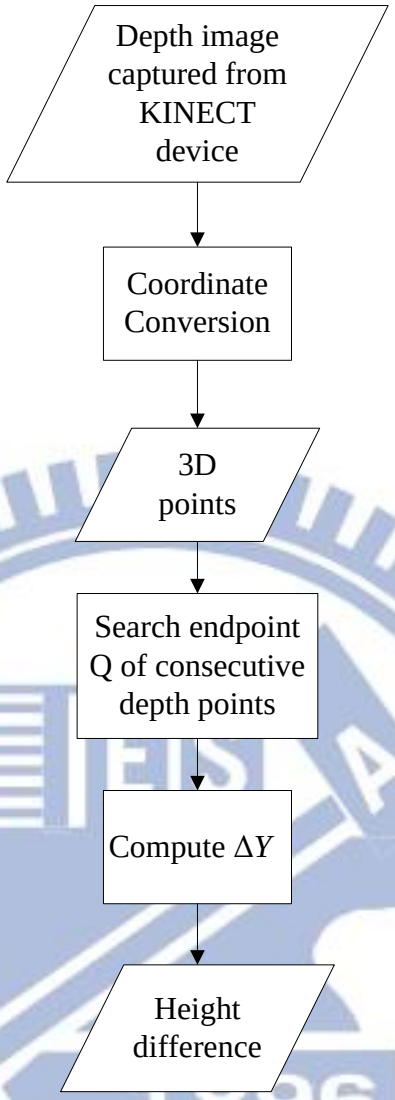

Figure 5.9 A flowchart of computing heights algorithm.

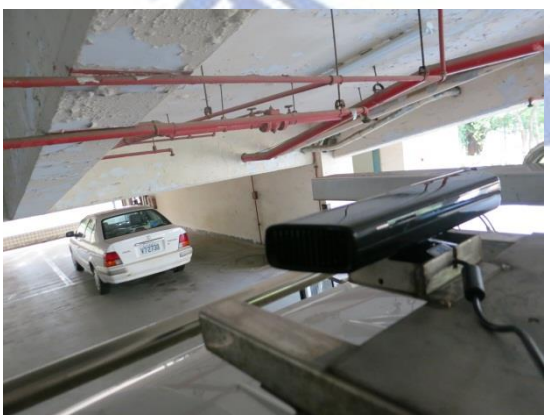

(a)

(b)

Figure 5.10 Monitoring the height-restricting barriers. (a) Seen from the front top of the car. (b) The computation result.

5.3 Collision Avoided Driving

5.3.1 Idea of Collision-free Driving

The most important thing in driving safety is to reduce the collision probability between cars. When an opposite car makes a right/left turn or a U-turn at an intersection, it might cause a car accident due to the lack of reaction time. If the driver notices the opposite car and slow down his/her own car earlier, the probability of getting into a car accident will be reduced. In order to achieve this aim, we propose a method for predicting the possible direction and movement of the opposite car by using the difference of monitored 3D information at an instant. With the prediction, the probability of collision can be lowered.

5.3.2 Predicting Algorithm and Experimental Results

In this section, the proposed scheme for predicting the possible direction and movement of the opposite car by using the difference of monitored 3D information at an instant is described. First, we acquire two sequential depth images and convert their coordinates into two groups of 3D points, respectively, by the coordinate conversion scheme described in Section 3.2.1. Next, let $P(x_1, z_1)$ and $Q(x_2, z_2)$ be the averages of the points in the two groups, respectively, which are just the centers of the groups, respectively. Then, the movement and direction of the object may be replaced by those of this center reduce computation time. Next, linear prediction is conducted. For this, at first a linear equation as follows is reviewed for use in the linear prediction:

$$Z = A \times X + B. \tag{5.5}$$

Then, we substitute the coordinates of each group center into Equation (5.5), respectively, to get:

$$z_1 = A \times x_1 + B; \tag{5.6}$$

$$z_2 = A \times x_2 + B. \tag{5.7}$$

The values of A and B may be computed by solving the simultaneous equations (5.6) and (5.7). And then we will have the linear equations which involve the centers P and Q. Finally, we check whether the linear equation intersects the border of the car as the prediction result. A schematic diagram is shown in Figure 5.11 and a flowchart of the prediction algorithm is shown in Figure 5.12. A detailed description of the algorithm is as follows.

Algorithm 5.3: predicting the possible direction and movement of the opposite car by using the difference of monitored 3D information at an instant.

Input: two sequential depth images d_1 and d_2 of the monitored car in front.

Output: the prediction result of the possible direction and movement of the opposite car.

Steps:

Step 1 Convert the coordinates of the depth images d_1 and d_2 into two groups G_1 and G_2 of 3D points, respectively, by the coordinate conversion scheme described in Section 3.2.1.

Step 2 Compute the averages $P(x_1, z_1)$ and $Q(x_2, z_2)$ of the points in groups G_1 and G_2 as the centers of the group, respectively.

Step 3 Compute the possible direction $V(x_v, y_v)$ and movement M of the opposite car by subtracting the coordinates of the center $P(x_1, z_1)$ from those of the center $Q(x_2, z_2)$.

Step 4 Compute the linear equation $f(x)$ which contains the centers P and Q by solving the simultaneous equations (5.6) and (5.7).

Step 5 Check whether the linear equation $f(x)$ intersects the pre-drawn border $g(x)$ of the car by solving the simultaneous equations $f(x)$ and $g(x)$ as the prediction result.

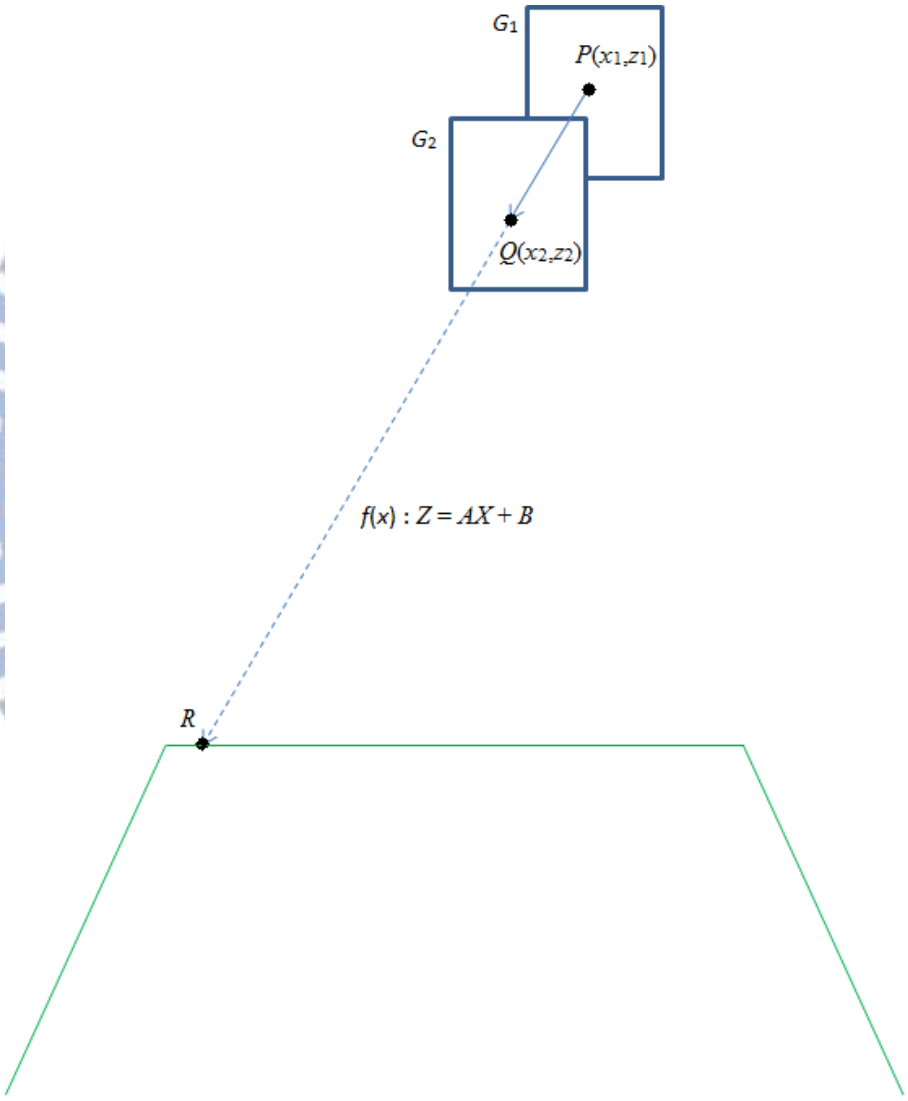

Figure 5.11 A schematic diagram of prediction algorithm.

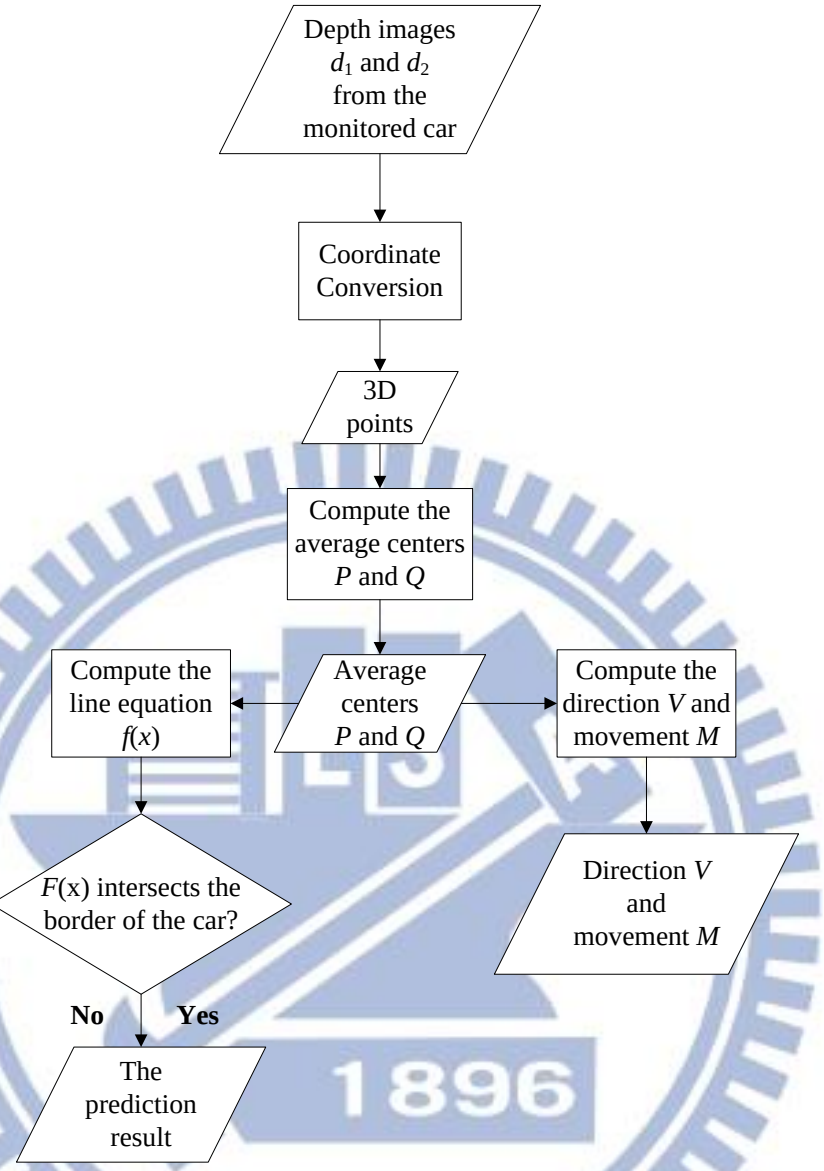

Figure 5.12 A flowchart of prediction algorithm.

In this experiment, a toy car is used to simulate the opposite car due to security concerns. Figure 5.13 shows an example of prediction. We can see the centers P of the opposite car, a line L which denotes the possible direction and movement of the opposite car, and an intersection R of the linear equation and the border of the car in Figure 5.13(a). Figure 5.13(b) shows the coordinates of the centers P, Q, the intersection R, respectively and a linear equation $f(x)$.

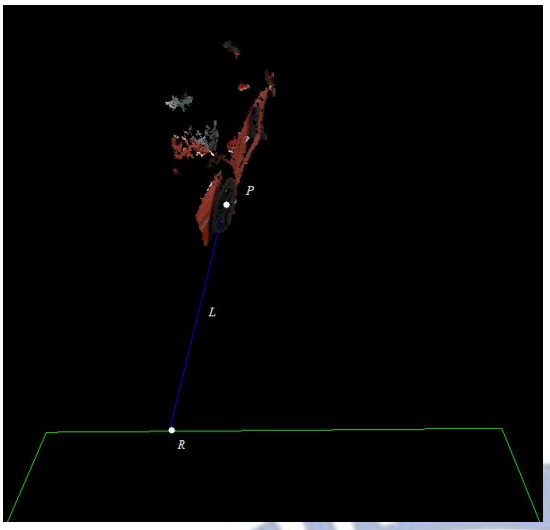

(a)

```
P ( -163.79, -712.246 )
Q ( -163.994, -707.143 )
R ( -192.248, 0 )
f(x) : Z = ( -25.0278) X + ( -4811.55 )
```

(b)

Figure 5.13 An example of prediction. (a) Models in 3D space. (b) Computation result.

Chapter 6
Experimental Results and Discussions

6.1 Experimental Results

In this chapter, experimental results of applying the proposed methods to 3D monitoring of car surrounds using the multiple KINECT devices affixed on the car mentioned in Chapter 2 are shown. The experiments were conducted in a parking lot and in the Computer Vision Lab in the Department of Computer Science at National Chiao Tung University.

The first experiment is modeling of a by-passing car using the 3D DWC as the tool for 3D image matching and registration. That is, we used the 3D DWC measure mentioned in Section 4.2.2 to overlap the car models constructed from different frames in order to compose a more complete model of the by-passing car. The second experiment is restoring car-accident scenes using the 3D DWC measure again. Due to security concerns, a toy car was used to simulate car accidents in this experiment. By the car models resulting from overlapping multiple 3D images by the use of the 3D DWC, it is feasible to restore a car-accident scene and check the responsibility in law. The third experiment is monitoring of ramps on the roads. In this experiment, we mainly used the KINECT device which is affixed in the front of the car and applying trigonometric functions and mathematical geometry to compute the slope of the ramp in front of the car. The last experiment is monitoring of limitations of heights of

constructs above the road. In this experiment, we used the KINECT device which is affixed on the front top of the car to monitor the height-restricting barrier and calculate the height difference between the car roof and the barrier.

A. Experimental Results of Modeling of a By-passing Car Using 3D DWC

In this experiment, the environment is an underground parking lot in National Chiao Tung University. A car passed through the left side of our car, as illustrated in Figure 6.1. The experimental result is shown in Figure 6.2, from which we can see that by overlapping more image frames, the constructed model of the by-passing car becomes more complete.

Figure 6.1 Illustration of a car passed through the left side of the video surveillance vehicle used in this study.

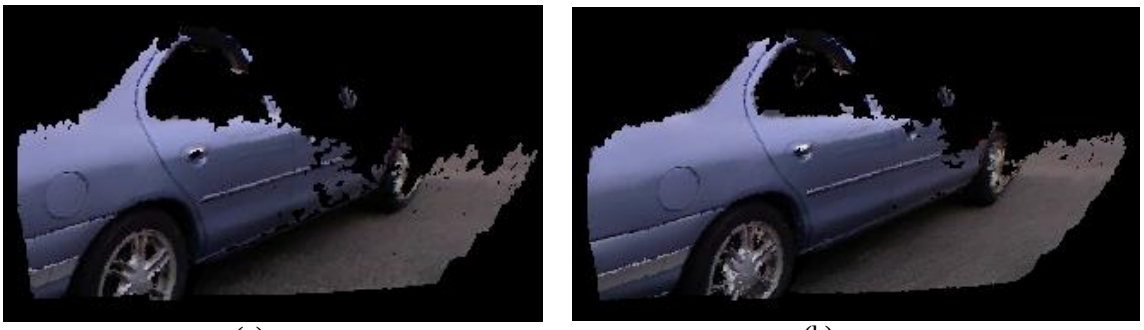

(a) (b)

(c)

Figure 6.2 The models of a by-passing car constructed by overlapping 3D images of different numbers of frames. (a) By one frame. (b) By five frames.(c) By ten frames.

B. Experimental Results of Restoring Car-accident Scenes Using 3D DWC

In the experiment for restoring car-accident scenes using the 3D DWC, we affixed three KINECT devices to a foam plank to simulate the front part of our car, as shown in Figure 6.3. A toy car moves right in the front and collides with our simulation car, as shown in Figure 6.4. The simulation results were shown in Section 4.4. Here, we show the full-scale simulation results in Figure 6.5 which shows the models of the involved car before the instant of collision by overlapping different numbers of frames, respectively.

C. Experimental Results of Monitoring of Ramps on the Roads

The environment for this experiment is a ramp in a underground parking lot in National Chiao Tung University. Firstly, the KINECT device affixed in the front of the car is shown again in Figure 6.6. Next, we drove the car to go through the ramp. We show the ramp in front of the car in Figure 6.7(a) and show the computed slopes of the ramp at different moments in Figure 6.7(b).

Figure 6.3 Three KINECT devices are affixed to the foam plank to simulate the video surveillance vehicle used in this study.

Figure 6.4 A toy car moves from right front and collides with the simulate car.

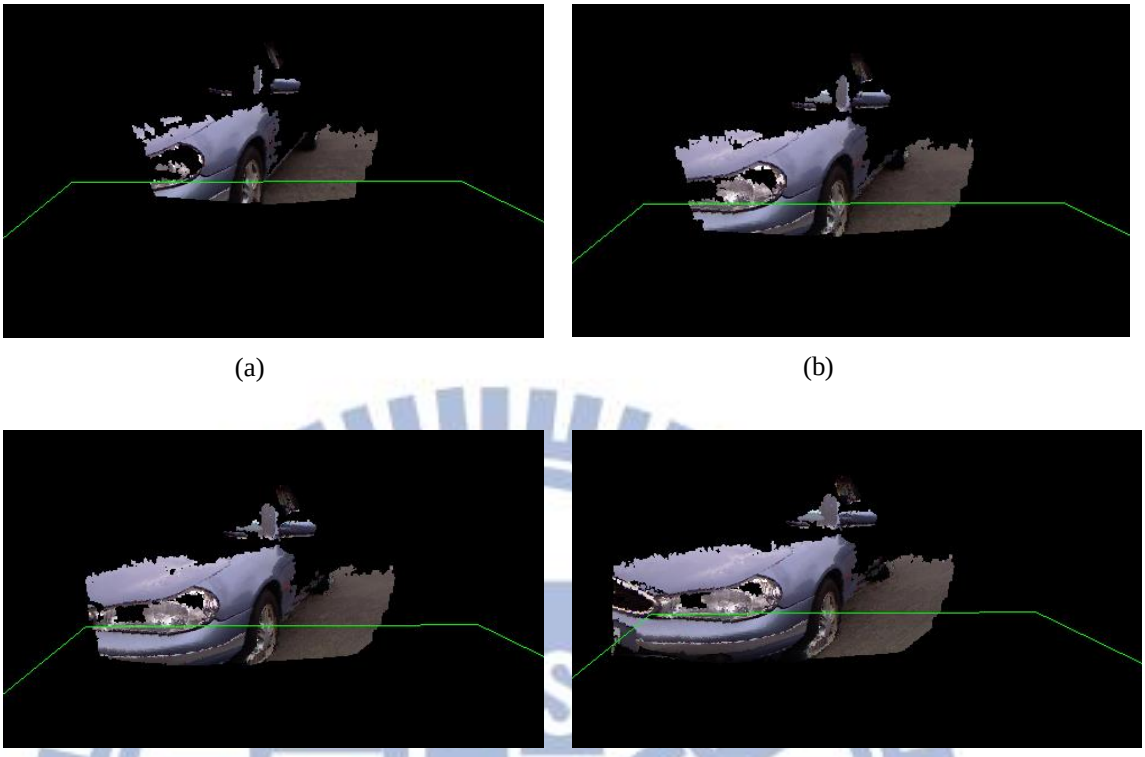

(a) (b)

(c) (d)

Figure 6.5 The models of an involved car before the instant of collision constructed by overlapping different numbers of frames. (a) With one frame. (b) With five frames.(c) With ten frames. (d) With fifteen frames.

Figure 6.6 The KINECT device affixed in the front of the car which is tilted down thirty degrees.

(a)

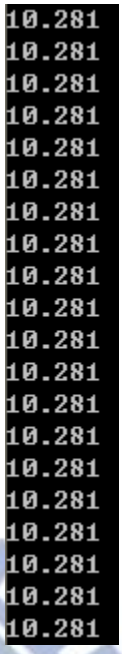

(b)

Figure 6.7 The experimental result on the ramp. (a) Front view from the car. (b) The computed values of the slope.

D. Experimental Results of Monitoring of Limitations of Heights on Roads

In the experiment for monitoring of limitations of heights on roads, we affixed a KINECT device to the front top of the car, as shown in Figure 6.8 and drove the car to a place with a limitation on the car height in the underground parking lot. In Figure 6.9(a), the relationship between the KINECT device and the height-restricting barrier is shown. In Figure 6.9(b), the computed values of the height difference are shown.

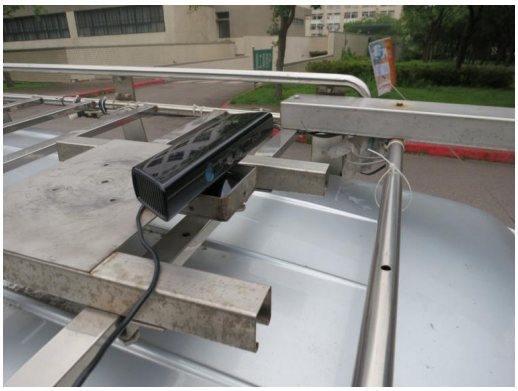

Figure 6.8 The KINECT device affixed on the front top of the car.

(a)

(b)

Figure 6.9 Results of monitoring height-restricting barriers. (a) Seen from the front top of the car. (b) The computation result.

6.2 Discussions

By analyzing the experimental results of 3D monitoring of car surrounds using the multiple KINECT devices, some problems are identified as follows.

(1) The precondition of using 3D DWC is that the models in any two sequential image frames need to be very similar, so the speed of the by-passing car cannot be fast. This condition may be relaxed if the program implementing the proposed method may be accelerated.

(2) Because 3D DWC includes multilayer loops, it will take a lot of time to compute the data of many frames. This problem may be solved by more efficient programs.

(3) Because the KINECT device sends the infrared light rays for depth sensing, other infrared light rays will interfere with the acquisition of depth information. The problem may be solved by taking images sequentially or by shutting off

other KINECT devices automatically while one KINECT device is working.

(4) If the height-restricting barriers were suspended from the ceiling, we might not acquire the depth information of the center point in the depth image. It will affect the computation of the desired height difference.

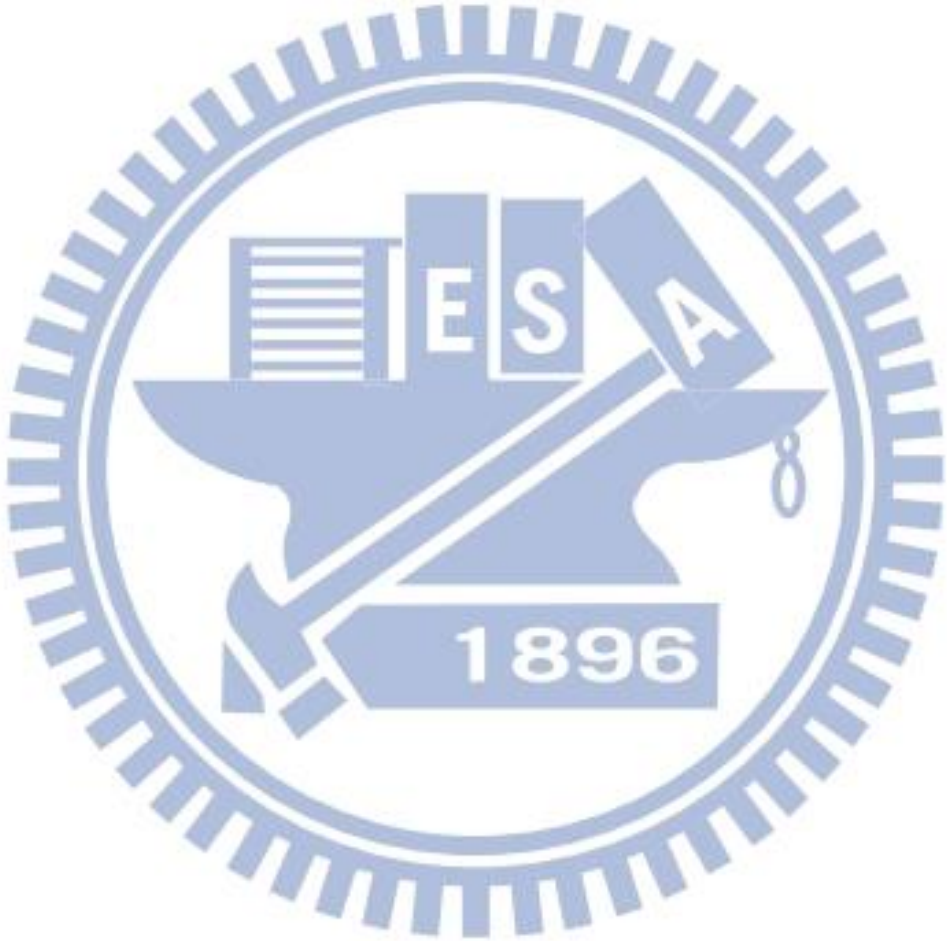

Chapter 7
Conclusions and Suggestions for Future Works

7.1 Conclusions

In this study, a system for 3D monitoring of car surrounds using multiple KINECT devices affixed on the body and top of a vehicle has been proposed. To implement such as a system, several methods have been proposed, as summarized in the following.

(1) *A method for coordinate conversion* based on the pinhole camera model has been proposed, which is employed to convert the coordinates of the depth image into 3D space points.

(2) *A method for geometric correction* has been proposed, which can be used to correct the bending phenomenon of a 3D image constructed from depth images acquired by KINECT devices.

(3) *A method for calibration between neighboring KINECT devices* based on the concept of the ICP has been proposed, which is used to stitch the images acquired by around-car KINECT devices into around-car 3D images.

(4) *A new measure of 3D DWC* based on the 2D DWC has been proposed, by which by-passing car models can be constructed and car-accident scenes can be restored.

(5) *Techniques for monitoring and computing parameters related to ramps and height-restricting barriers* has been proposed, which uses trigonometric functions and mathematical geometry to measure the slope of the ramp and calculate the

height difference between the car roof and the barriers for pre-warning of dangerous conditions during road driving.

(6) *A method for predicting the possible direction and movement of the opposite car* has been proposed, which can be used to increase to pre-warn possible car accidents to achieve safe driving.

The experimental results described in the previous chapters show the feasibility of the proposed methods.

7.2 Suggestions for Future Works

According to the experience obtained in this study, some suggestions and related issues which are worth further investigating in the future are listed in the following.

(1) It is desired to speed up the calibration process to reduce the preparation time before using the system.

(2) It is desired to find a new method of coordinate conversion which is more accurate than the pinhole camera model.

(3) It is desired to find a new method of correction which is more accurate than geometric correction.

(4) It is a challenge to speed up the computation of the 3D DWC measure to reduce the execution time.

(5) It is a challenge to find more accurate predictions of car accidents than the linear prediction scheme adopted in this study.

(6) It seems necessary to embed KINECT devices into the car body to avoid being destroyed during driving.

References

[1] C. Scharfenberger, S. Chakrabotry, and G. Farber, “Robust image processing for an omnidirectional camera-based smart car door,” *Proc. IEEE/ACM/IFIP 7th Workshop on Embedded Systems for Real-Time Multimedia*, 2009.

[2] T. Gandhi and M. M. Trivedi, “Vehicle surround capture: survey of techniques and a novel omni-video-based approach for dynamic panoramic surround maps,” *IEEE Trans. Intelligent Transportation System*, vol. 7, no. 3, pp. 293-308, Sep. 2006.

[3] S. Acharya, C. Tracey, and A. Rafii, “System design of time-of-flight range camera for car park assist and backup application,” *Proc. IEEE Computer Society Conference on Computer Vision and Pattern Recognition Workshops*, 2008, pp. 1-6.

[4] Y. C. Liu, K. Y. Lin, and Y. S. Chen, “Bird’s-eye view vision system for vehicle surrounding monitoring,” in *Lecture Notes in Computer Science*, vol. 4931, G. Sommer, R. Klette, Eds. Springer Berlin/Heidelberg, 2008, pp. 207-218.

[5] Chaiyawatana, N., Uyyanonvara, B., Kondo, T., Dubey, P. and Hatori, Y., “Robust object detection on video surveillance,” in Computer Science and *Software Engineering (JCSSE)*,2011,pp. 149-153.

[6] Techbang, “Kinect for Windows Sensor Components and Specifications,” http://www.techbang.com/posts/2936-get-to-know-how-it-works-kinect.

[7] Pavankumarvasu, “Programming KINECT in C++ and OpenGL — Mapping Color and Depth Streams, ” http://pavankumarvasu.wordpress.com/programming-kinect-in-c-and-opengl-ma

pping-color-and-depth-streams.

[8] Wikipedia, “Pinhole camera model, ”, March 2013. http://en.wikipedia.org/wiki/Pinhole_camera_model.

[9] B. C. Ma and W. H. Tsai. “3D Environment Modeling and Monitoring via KINECT Images for Video Surveillance,” Master Thesis, National Chiao Tung University, June 2013. Institute of Computer Science and Engineering College of Computer Science.

[10] Wikipedia, “Iterative closest point, ”, May 2013. http://en.wikipedia.org/wiki/Iterative_closest_point.

[11] T. C. Fan and W. H. Tsai (1984). "Automatic Chinese seal identification," Computer Vision, Graphics, and Image Processing, Vol. 25, pp. 311-330.